

# CHAPTER 1

## INTRODUCTION

This chapter will highlight the background study, problem statement, the main objectives of the work, scope of study and also significance the project.

### 1.1 BACKGROUND STUDY

A solar chimney is a device that can be used commonly for ventilation or as a renewable energy power plant. In this study, the solar chimney which normally only utilizes solar thermal energy will be incorporated into a plant that produces flue gases. The thermal energy from sun radiation and flue gases will be heat sources that will increase temperature of the air within the chimney. The hot air will create an updraft air in the chimney that will then escape into the atmosphere. The updraft air will shear the blades of the circular wind turbine and the rotating blades will form rotational energy that will be converted into electrical energy via a generator [1]. The circular wind turbine will be housed in a circular chimney (figure 1.1).

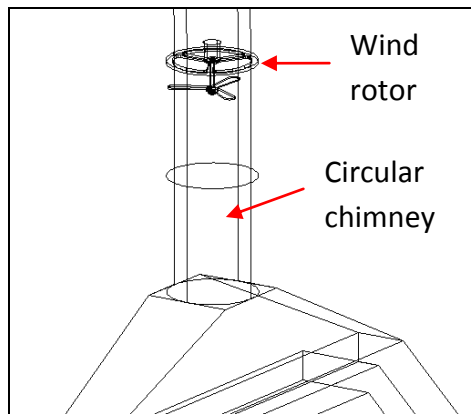


Figure 1.1: Circular chimney and wind rotor.

## **1.2 PROBLEM STATEMENT**

A solar chimney backed up with flue gases as an alternative heat resource was designed and fabricated. The purpose of the flue gases is to substitute the solar energy as a heat source which only occur 12 hours a day, especially during at night, cloudy or rainy days when the sun is not present [2]. The wind turbine rotor used initially was Savonius type supported by a rectangular cross section chimney.

Experiments were conducted but the analysis showed that the arrangement (Savonius and chimney) were not appropriate as it yielded a low efficiency [3]. The rotor proposed is to be replaced with a traditional circular rotor (propeller type) supported by a circular cross section chimney which will attempt to increase the efficiency of the solar chimney.

## **1.3 OBJECTIVES**

The objectives that have been identified to be achieved at the end of the project completion are as follows:

- a. To re-design and fabricate a new chimney to house circular wind turbine replacing the Savonius rotor.
- b. To modify the plate of the collector to a finned gas-to-gas heat exchanger based on analytical evaluation.
- c. To conduct experimental measurements under the solar mode operation, flue gas mode operation and hybrid mode for two types of blades.

## **1.4 SCOPE OF STUDY**

There are four scopes of studies for this experiment. One of them will be the fabrication of a circular wind turbine. In order to design and fabricate a circular wind turbine to replace the original Savonius rotor, research is done on rotor-dynamics.

Secondly is to design a new turbine casing unit, or the chimney, in order for it to accommodate the new circular turbine via a CAD program to ease dimensional alterations.

The glass panel will be painted black to enhance thermal energy absorption and experimental measurements that account for solar mode generation will be acquired [5].

## **1.5 SIGNIFICANCE OF WORK**

Power generation is constantly known as one of the biggest challenges human face in this era. Conventional power generation not only consumes precious fuels, at the same time, it contributes pollutants and increased temperature to the environment.

The present work, if a commercialized model is built and operational, it will not only increase the efficiency of power generation, it also contributes economically, indirectly reducing pollutants generation, and ultimately reduce the warming of atmosphere (the green house effect) caused by flue gasses discharge from thermal power plants.

## **CHAPTER 2**

### **LITERATURE REVIEW**

This section will elaborate more about elements that are involved in this study. The elaborations are supported by quotations from paper studies, websites, books or journals.

#### **2.1 FLUE GAS UTILIZATION**

Flue gases are produced when coal, oil, natural gas, wood or any other fuel is combusted in sources such as an industrial furnace, a power plant's steam generating boiler, or other large combustion device (some examples in figure 2.1).

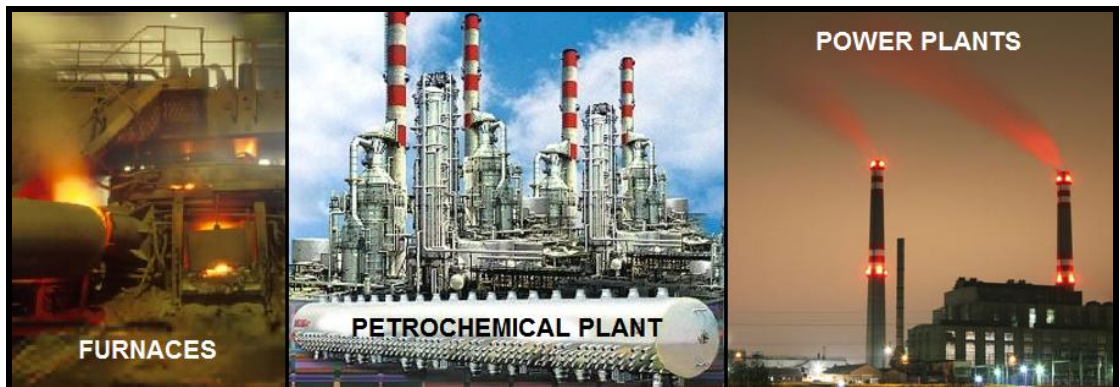


Figure 2.1: Flue gases sources

Basically, as flue gases are released from, for example, power plant system to the environment commonly via stacked chimneys, it contains a fairly large untapped potential of thermal energy. Often a considerable economical advantage can be achieved by cooling the flue gas, and thereby utilizing the energy amount, which under normal circumstances would have been let out as heat loss [5].

Figure 2.2 shows the electrical power generation potential from waste heat recovery by EIA 2007 Annual Energy Outlook. Besides being considered for use in this application of hybrid solar chimney, according to WOW energy on their presentation in AIChE Chicago Symposium 2007, flue gases have been utilized in applications such as WOWGen’s combined cycle turbo expander system for solar, biomass and geothermal plants. For low temperature energy extraction, single stage turbo-expanders are utilized. The mentioned applications require use of a very efficient flue gas heat exchanger.

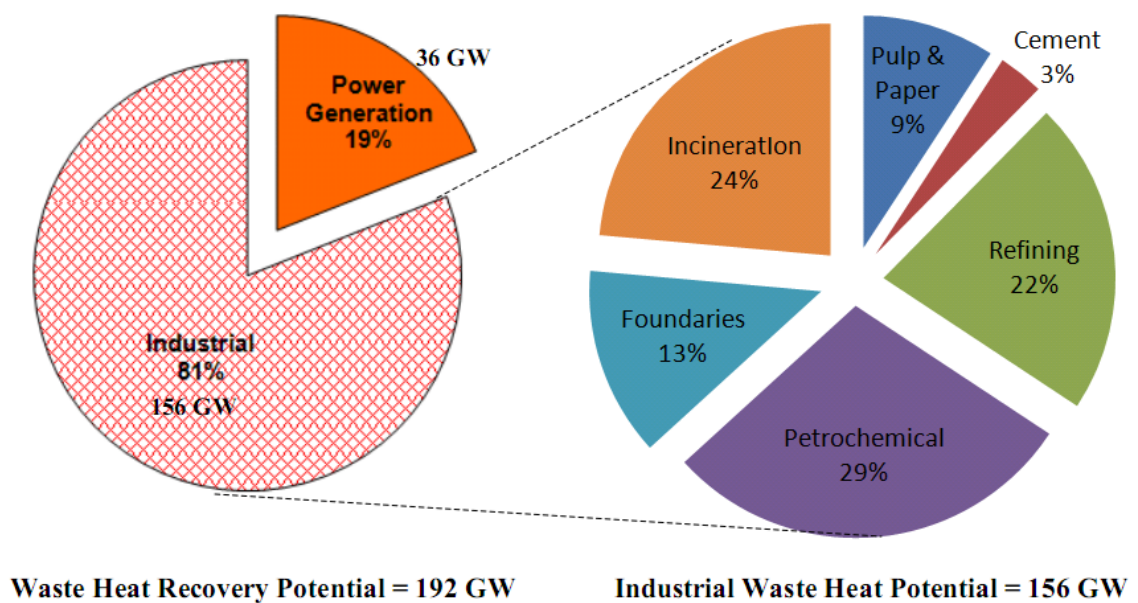


Figure 2.2: Electrical power generation potential from waste heat recovery.

Source: WOW energy presentation, AIChE Chicago Symposium 2007

Some of the industries have already started manipulating the energy recovery of flue gases for economic and environment purposes. For example, in a paper sludge industry, in addition to the incinerator, a natural circulation water tube boiler is used to effectively recover steam from the waste heat of the flue gas [6].

## 2.2 GAS TO GAS HEAT EXCHANGERS

A heat exchanger is a device built for efficient heat transfer from one medium to another, whether the media are separated by a solid wall so that they never mix, or the media are in direct contact [7]. In this study, we are using the application of the heat exchanger, but between two gas mediums; the flue gases in the flue gas passage and the air in the air passage. Heat will be transferred from the flue gases via a heat exchanger to heat up air in the air passage (figure 2.3).

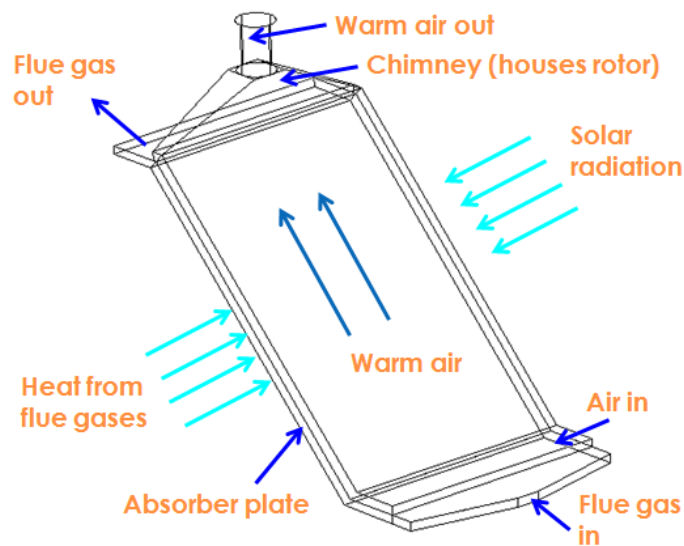


Figure 2.3: Gas to gas heat exchanger principle on hybrid solar chimney.

The transfer of heat from one process' gas to another process' gas is done in a gas-to-gas heat exchanger. A compact gas to gas heat exchanger needs large heat transfer areas on both fluid sides. Gas to gas heat exchangers usually take the form of a vertical shell and tube heat exchanger. Variations of the standard design are horizontal units, plate type heat exchanger and heat exchangers that are located inside the converter vessel [8].

### 2.3 EXTENDED SURFACES

According to Incropera et al, 2007, extended surfaces are commonly used to depict a case involving heat transfer by conduction within a solid and heat transfer by convection (or radiation) from the boundaries of the solid [9]. There are many situations that involved such combined conduction and convection effects, where the most frequent application is one in which extended surfaces are used to enhance heat transfer between a solid and a fluid, called fins.

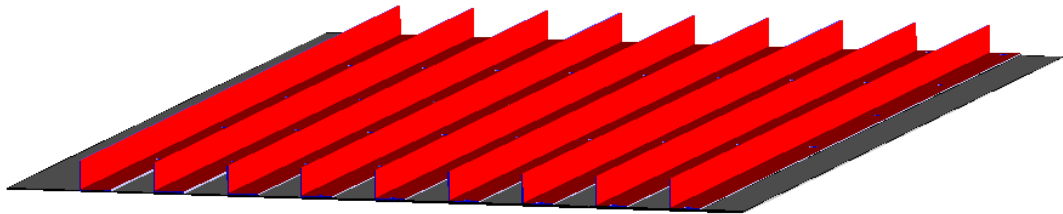


Figure 2.4: Extended surfaces (fins) to enhance heat transfer.

Large heat transfer areas can be achieved by adding secondary surfaces. The secondary surfaces are such as plate fins, strip fins, and louvered fins. The fins extend the heat transfer surfaces and promote turbulence [10]. Most gas to gas heat exchangers imply the use of extended surfaces because they promote optimum heat transfer.

The thermal conductivity of the fin material has a strong effect on the enhancement of the heat transfer of a fin [11]. A figure shown above is an example of a finned surface (figure 2.4):

## 2.4 FLAT COLLECTOR AND ABSORBER PLATES

A typical flat-plate collector is a metal box with a glass or plastic cover on top and a dark-colored absorber plate on the bottom. The glass or plastic cover on top is normally called glazing [12]. In this study of the solar chimney, the flat plate collector is a metal box with a plastic (Perspex) cover top. The conventional absorber plate is actually made of corrugated aluminum, of which will be removed and modified to an aluminum finned absorber plate.

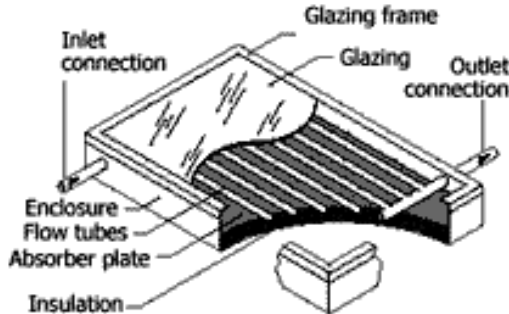


Figure 2.5: A typical flat plate collector with absorber.

According to Prakash and Garg, 2000, absorber plates should have high thermal conductivity, adequate tensile and compressive strength and good corrosion resistance [13]. That is why in this study, aluminum is considered as they are commercially available and cheap. Fins are installed on the aluminum absorber plate to increase heat transfer. The calculations and theoretical design of this finned absorber plate is highlighted in chapter 4 in this report.

Balbir and Fauziah showed that the thickness of the absorber plate should not be more than 2 mm as daily efficiency will be constant even with increasing plate thickness [4]. A general picture of a flat plate collector is shown in figure 2.5.

## 2.5 WIND TURBINES

In this study, a similar application of the wind turbine is incorporated into the solar chimney in order to realize efficient power generation. Basically, wind turbines are designed to exploit wind energy [14]. A Horizontal Axis Wind Turbine (HAWT) installation consists of sub-systems to catch the wind's energy, point the turbine into the wind, and convert mechanical rotation into electrical power. A classic modern blueprint of a modern wind turbine is shown in figure 2.6 below:

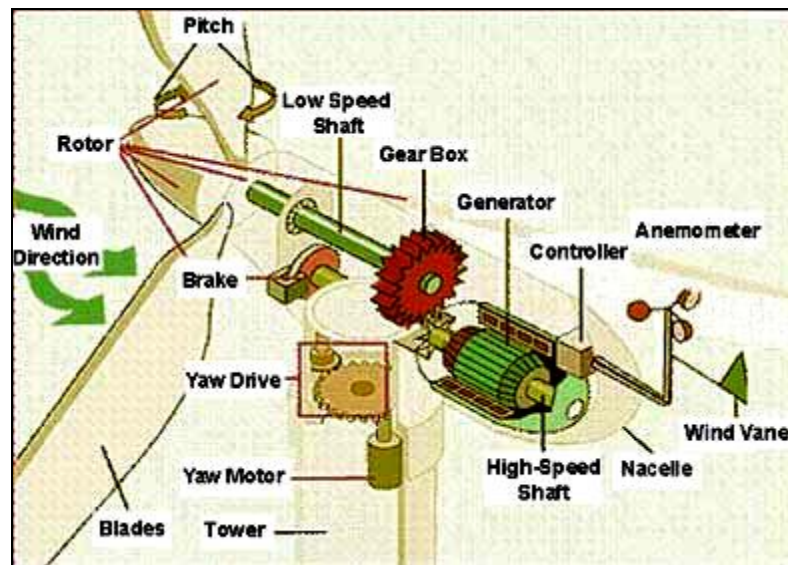


Figure 2.6: Classic blueprint of a modern wind turbine.

Source: [www.energybible.com](http://www.energybible.com)

Similar to the application to the hybrid solar chimney, the propeller will be installed vertically facing downwards on the chimney and hot air that is induced by the heat transfer of either the flue gases or solar energy will shear the blades of the propeller as it is naturally driven up the chimney. The rotational motion of the propeller will then drive a generator that will produce electricity.

## 2.5 SOLAR CHIMNEY ENHANCEMENT

The conventional solar chimney design is not perfect and thus improvements can be done to enhance the capability of a solar chimney. According to Alan, 2007, suitable dimensions are very important such as the diameter of the throat to achieve highest velocity as well as height of the chimney to increase the efficiency of the chimney [9].

Referring to figure 2.7, the smaller the throat diameter is, the higher the exit velocity of the wind. The faster exit velocity of the air will induce low pressure, according to Bernoulli's correlation and that is favorable. The low pressure region at the nozzle of the chimney creates a natural air upwards drive.

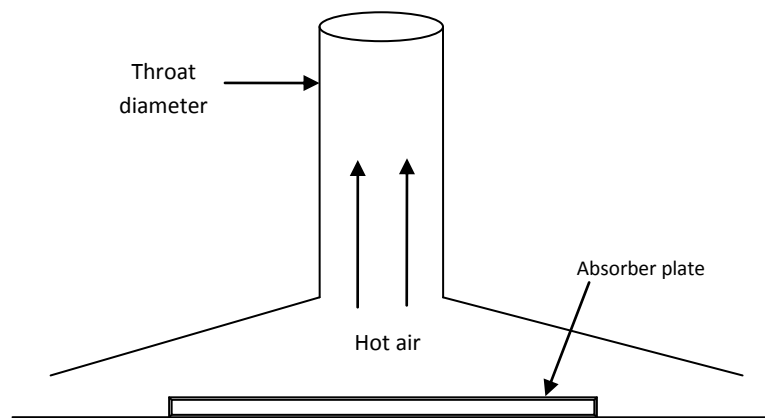


Figure 2.7: Conventional solar chimney design.

According to Padki and Sherif, 1999, enhancement can be done to reduce the height of the chimney by reducing the outlet area [15]. The following figure 2.8 depicts a radically different geometry of the chimney:

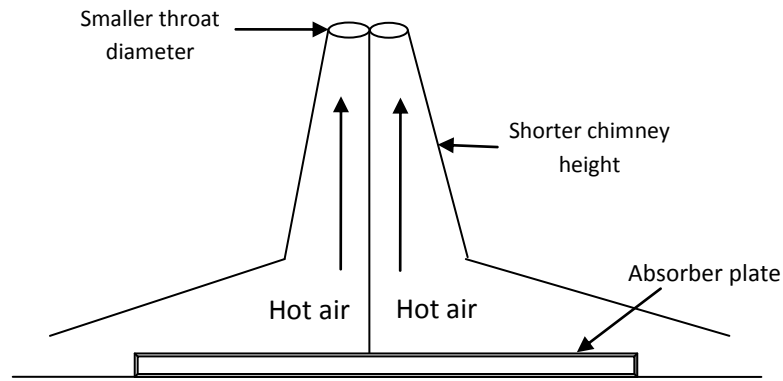


Figure 2.8: Enhancement on solar chimney (reduced height).

Another radical change that is proposed by Alan, 2007 is shown in figure 2.9 [9]. The different slopes of the collector and chimney are brought into one integral structure which will resemble a large conical shape. The solar absorber is placed inside the base of the cone to allow highly efficient heat transfers to the air flow. The third critical difference is that the turbine is at the top of the chimney/nozzle where the velocity of the air flow is greatest.

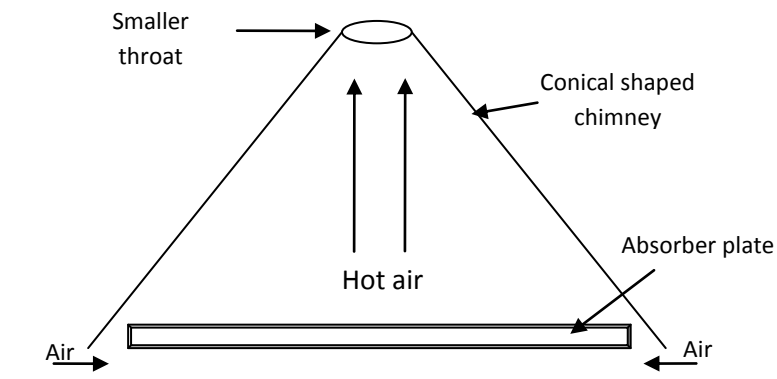


Figure 2.9: Conical geometry of enhanced solar chimney.

## **CHAPTER 3**

### **METHODOLOGY**

This section covers the analysis technique, the project execution flow chart, and also the full FYP I and FYP II Gantt Charts that are essential for smooth execution of this project.

#### **3.1 ANALYSIS TECHNIQUES**

The methodologies that will be exercised throughout the project are as follows:

- a. Analytical.
- b. Model modification and fabrication.
- c. Experimental measurements.

#### **3.2 EXECUTION / FLOW CHARTS**

The following flowchart (figure 3.1) depicts procedures that are done as the project progresses/modified or troubleshooting is done as problems surface. This flowchart is more specific and it is basically detailed procedures that are in the middle of the overall execution flow chart (figure 3.2).

The fin design and calculations, absorber plate improvements, and chimney design improvements procedures are based on the progress/troubleshooting flowchart (figure 3.1) below:

Figure 3.1: Execution / Troubleshooting flowchart.

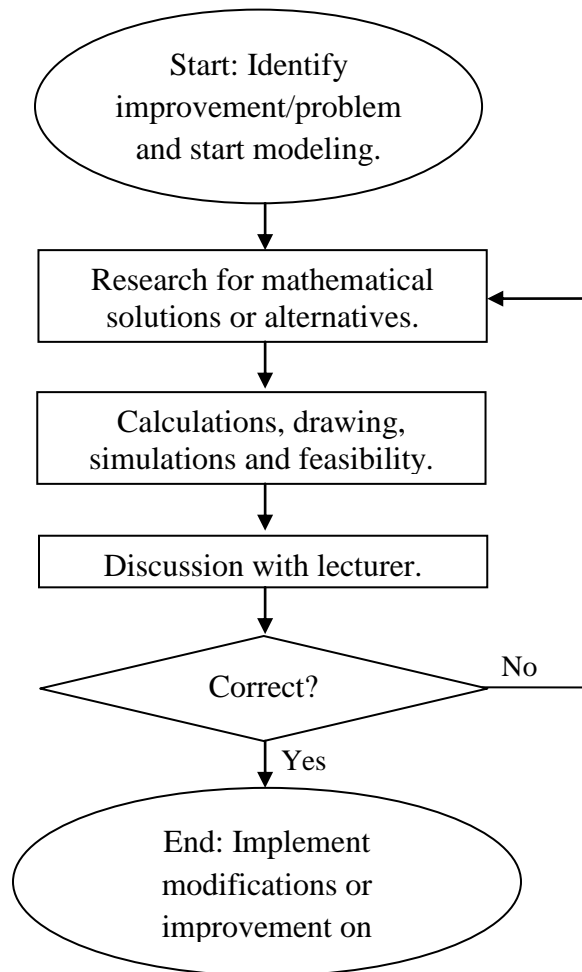
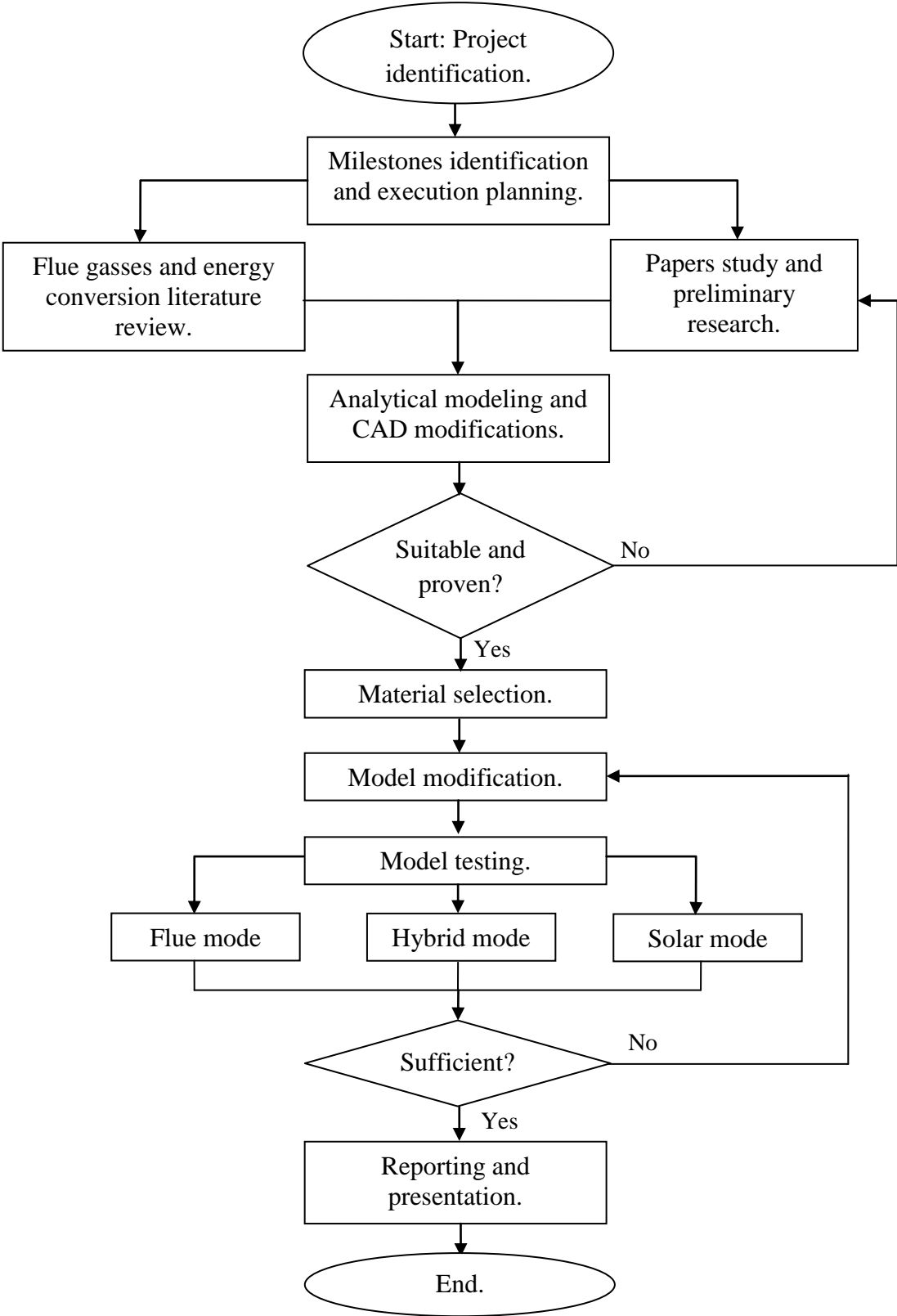


Figure 3.2: Overall execution flow chart



### 3.3 GANTT CHART FOR FYP I

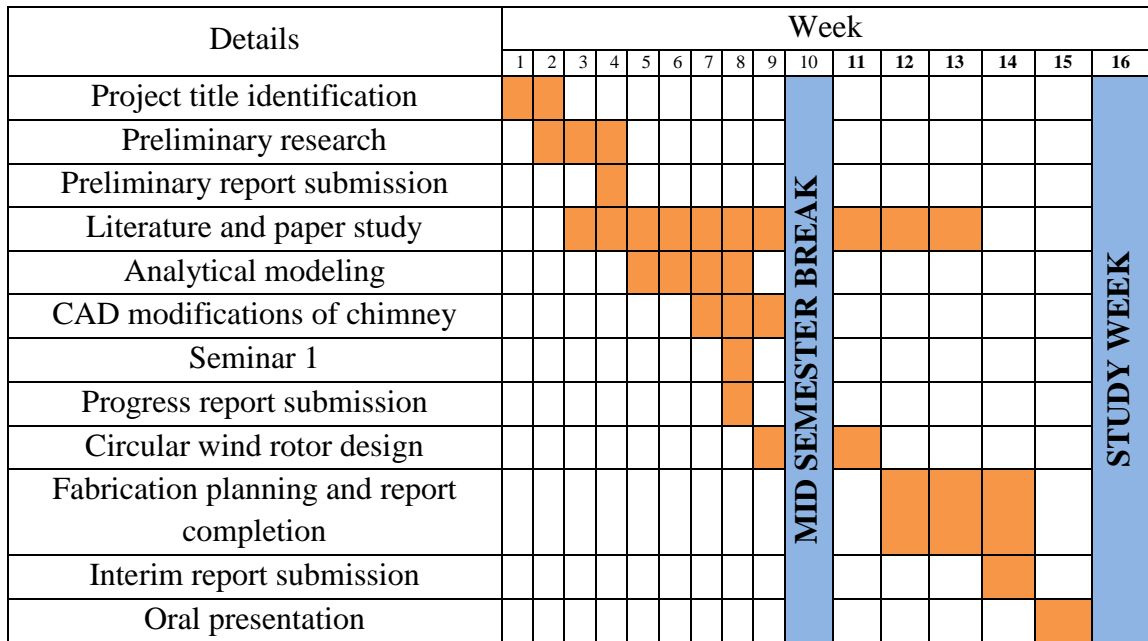


Figure 3.3: Gantt chart for FYP I.

### 3.4 GANTT CHART FOR FYP II

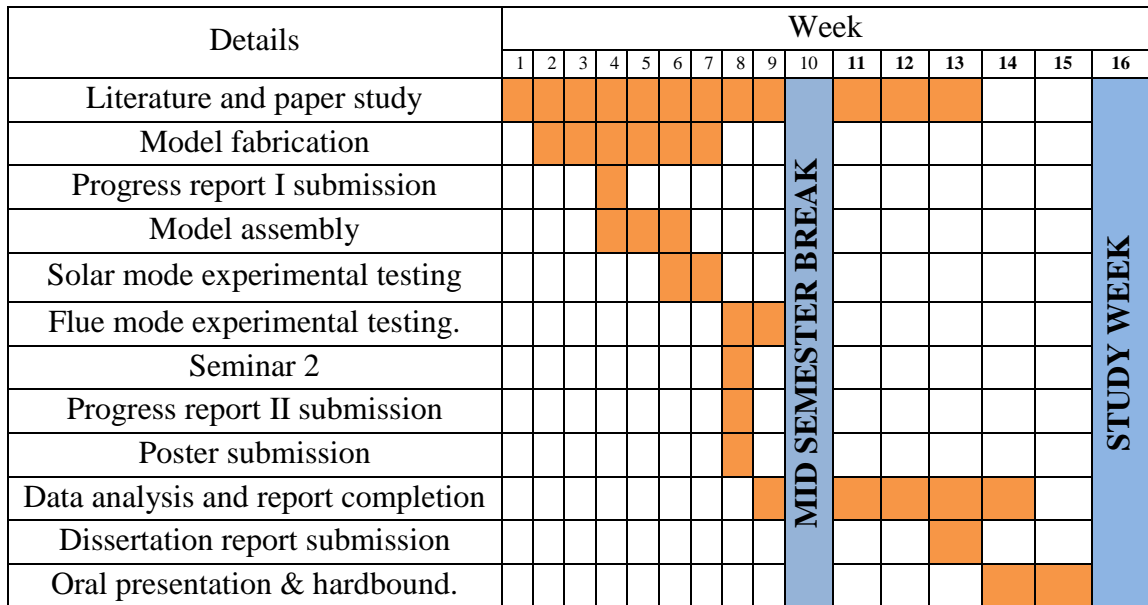


Figure 3.4: Gantt chart for FYP II.

## **CHAPTER 4**

### **CONCEPT OF MODIFICATION**

In this section, some major physical improvements are highlighted and comparison between the conventional design and the improved design of the solar chimney are calculated and proven theoretically.

#### **4.1 MODEL MODIFICATION**

The fabricated model must be physically modified to increase the efficiency of the overall hybrid solar chimney compared to the conventional one using the Savonius rotor with a rectangular chimney.

##### **4.1.1 Absorber plate**

The current design of the absorber plate is a corrugated plate. The corrugated plate has increased area compared to a flat plate, which will allow more heat transfer as there will be more contact between the flue gasses and absorber plate but the heat transfer rate can still be boosted by further increasing the area of contact, which can be implemented via a finned absorber plate [11].

The finned aluminum absorber plate will be fabricated in the university with limited cost and facilities and thus the design will be fairly simple. Nine angled aluminum, which will be the fins, will be attached to a 1 x 1.5 meter flat aluminum plate via screws evenly. The fins dimensions are as figure 4.1, in centimeters.

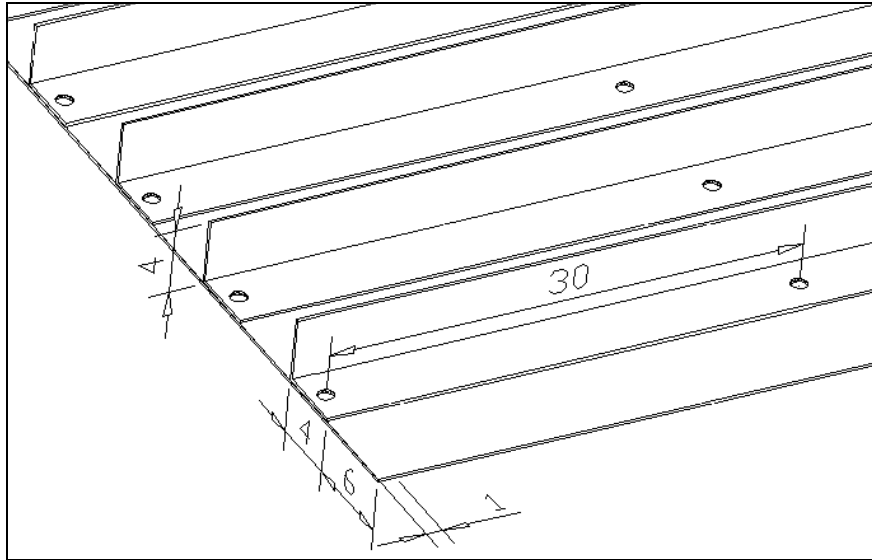


Figure 4.1: Finned absorber dimensions, in cm.

#### 4.1.2 Chimney

In order to house the circular wind rotor and the generator, the conventional chimney that houses the Savonius rotor must be removed and a new circular chimney must be fabricated and installed. The modifications will be based on the ability of the chimney to house the generator and the blades.

The new fabricated circular chimney is shown in figure 4.2. A small incline in the construction of the chimney is to accommodate a large 6 inch diameter PVC pipe chimney. The 6 inch pipe diameter, which will also be the generator housing, will extend vertically for 1 meter and then followed by reducer connected to a 4 inch PVC pipe which will increase the height of the chimney by 2 meters (figure 4.3).

A smaller air passage exit will increase the Bernoulli Effect [16]; increased velocity at the air exit, reducing pressure and hence increasing air velocity of air moving updraft inside the passage.

A diameter of 6 inches has been chosen for the chimney because the particular size is a common measure commercially. Besides, in order to reduce the frictional loss caused by gears and consideration of gear ratios, the generator will be mounted inside the chimney itself, taking advantage of the large chimney size of 6 inches in diameter.

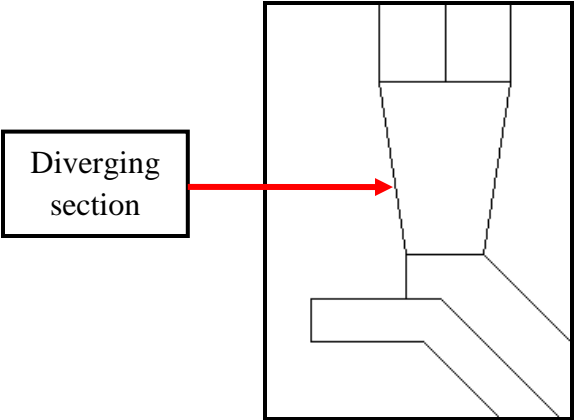


Figure 4.2: Divergence to support large 6 inch diameter PVC pipe.

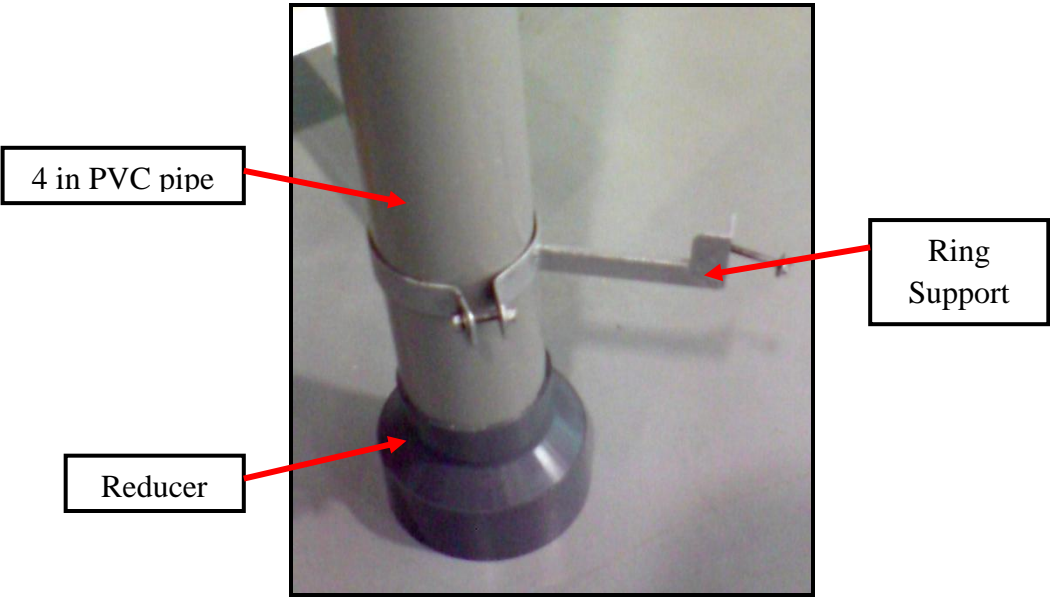


Figure 4.3: 4 inch PVC pipe with reducer and height support.

### 4.1.3 Generator Housing

As mentioned in the previous section, the 6 inch pipe diameter will house the generator housing. A generator support is fabricated using Perspex due to durability and flexibility in fabrication. The generator support is attached to the generator using screws to prevent vibrations during propulsion of the propellers. The generator support is mounted to the 6 inch PVC pipe by sliding it into a smaller support in the pipe (figure 4.4).

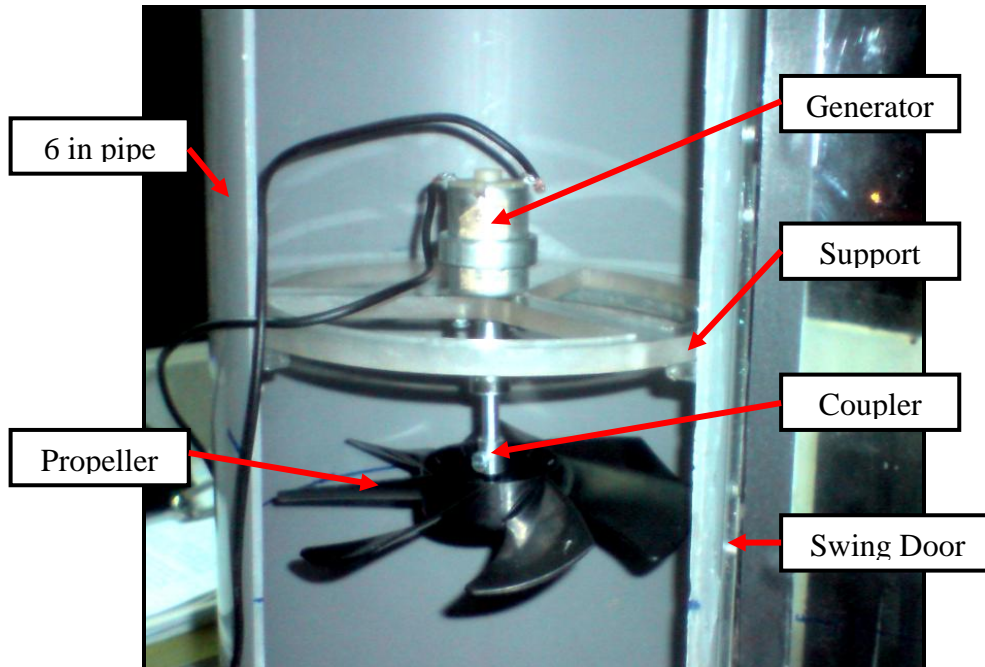


Figure 4.4: Generator housing in 6 inch PVC pipe.

An aluminum coupler is fabricated using the lathe machine in order to connect the generator shaft to the propeller shaft easily. This coupler too allows interchangeable propellers during maintenance or operations. A more detailed generator assembly can be seen in figure 4.5.

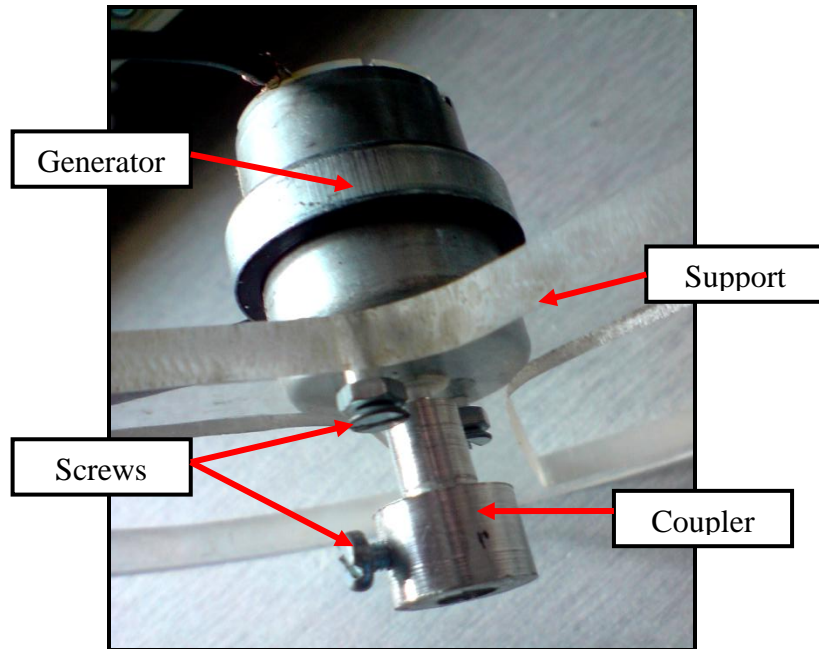


Figure 4.5: The generator assembly.

As S. Mathew noted, a smaller conduit allows the wind energy to transfer into electrical energy more efficiently [18]. A suspended generator that holds the wind rotor vertically as shown in figure 4.4 actually mimics a conventional power generating wind turbine tower. The only difference is that the generator and the motor are placed vertically instead of horizontally due to wind direction.

#### 4.1.4 Body

A few enhancements to the Hybrid Solar Chimney's body were done in order to increase the efficiency of the entire system significantly. A research simulation of the same study shows that by enlarging the air passage inlet, the volume of air going into the air passage will be increased.

There is a certain threshold to the height of the air passage inlet because too wide an opening will cause air recirculation in the passage and decreases the efficiency of the system. The height of the opening was increased from 9 cm to 16 cm (figure 4.6).

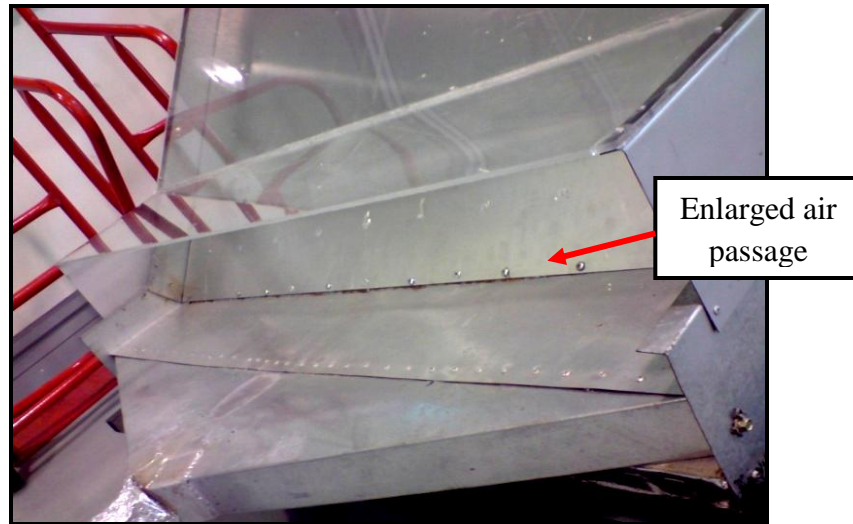


Figure 4.6: Increased height of air passage.

A rain cover (figure 4.7) was also installed to the top of the chimney to allow the model to be used outdoors. The rain cover is to discourage rain water to enter the chimney and wet the generator housing assembly.

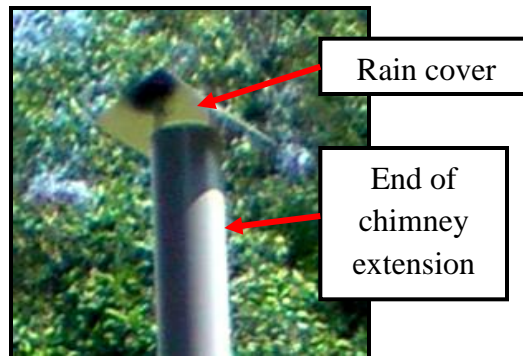


Figure 4.7: Increased height of air passage.

#### 4.1.5 Support

As the chimney exit is conventionally 5cm x 1m in size, the chimney will have to diverge in size to house the 6 inch circular pipe. The chimney exit was enlarged to 3 inches to support the diverging system of the chimney.

The diversion may cause instability to the whole chimney and the whole model might just give way and collapse. Due to that, thus, rigid supports are essential to provide a better rigid support to the tall chimney and also to prevent vibration during operation.

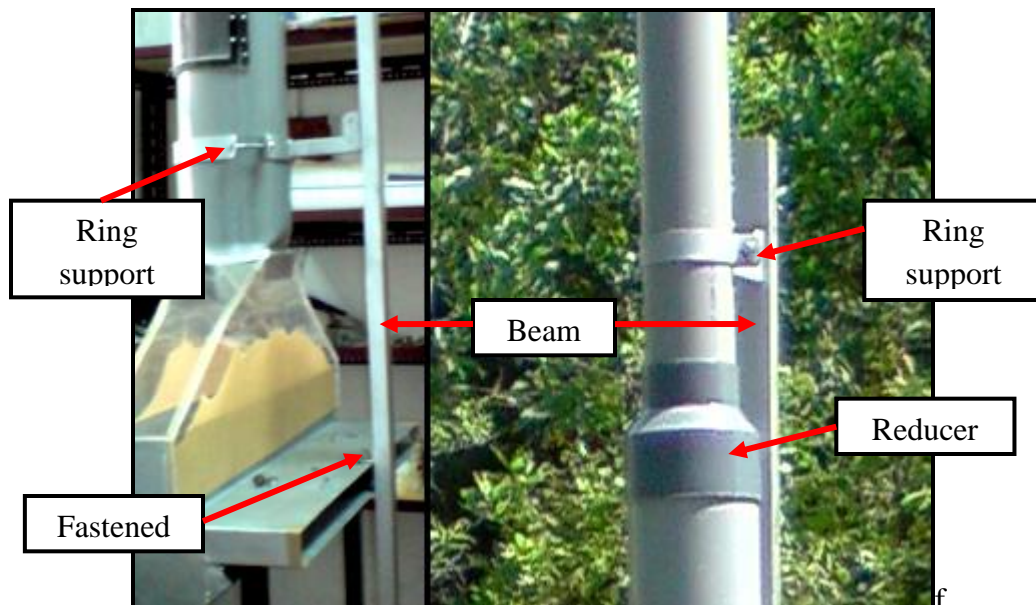


Figure 4.8: Chimney support design.

A tall beam is installed into the base of the model and enforced into the flue gas outlet. The 6 inch and the 4 inch PVC pipe will be installed with a mechanism that will be attached to the beam as support. The end result is a sturdy and rigid model even though there is a 3 meter chimney extension.

#### 4.1.6 Paint Selection

Material	Absorptivity, $\alpha$	Emissivity, $\epsilon$	Performance Factor, $\alpha/\epsilon$
Black chrome on copper	0.95	0.12	7.92
Nonmetallic black surfaces: carbon	0.92	0.94	0.98
Black paint	0.97	0.86	1.13
Gray paint	0.75	0.95	0.79

Source: Michael Modest, 2003, Radiative heat transfer, Amsterdam : Academic Press, Oxford Universiti Press

The objective to paint the absorber surface with non glossy dark coloured paint (figure 4.9) is to achieve maximum absorptance,  $\alpha$  and minimum re-emittance,  $\epsilon$  so that the ratio of performance factor,  $\alpha/\epsilon$  is a maximum [17]. The black non glossy paint is selected for coating because it is locally available and cheap compare to black Nickel or black Chrome on copper.



Figure 4.9: Black painted absorber plate.

#### 4.1.7 Wind Rotor

The fabricated wind rotors are as shown in figure 4.10. Two sets of experiments will be conducted using both rotors in the flue gas and solar mode experiments. The propeller is 4 bladed (left) while the multi bladed rotor has 7 blades. The experiments are to determine the efficiency of the blades in a low humidity close conduit flow.



Figure 4.10: The propeller (left) and the multi bladed rotor (right).

After the experiment, there was not enough wind velocity to induce propulsion to test the efficiencies of the wind rotor. Thus the wind rotors are kept for further research proposes in the future.

## 4.2 HEAT TRANSFER ANALYSIS OF FINNED ABSORBER

The heat transfer analysis is important for this study to calculate the theoretical heat transfer of the model to see the theoretical efficiency of the model.

### 4.2.1 Basic parameters and dimensions

A summary of the thermo physical properties of flue gases from a gas turbine power plant at a temperature of 850 K are tabulated in table 4.1 [3] and the basic parameters of the solar chimney in table 4.2:

Properties of flue gases	Gas turbine power plant at T = 850 K
Density, $\rho_{fg}$ (kg/m <sup>3</sup> )	0.43
Specific heat, $C_{p,fg}$ (J/kg.K)	1242.96
Viscosity, $\mu_{fg}$ (kg/m.s)	0.000034
Thermal conductivity, $k$ (W/m.K)	0.056
Prandtl Number, $Pr$	0.76

Table 4.1: Thermo physical properties of flue gases.

Dimensions	Formula	Values
Inlet cross sectional area, $A_c$ (m <sup>2</sup> )	$L \times W$	0.05
Hydraulic diameter, $D_H$ (m)	$4A_c/P$	0.095
Wetted parameter, $P$ (m)	$2L+2W$	2.1

Table 4.2: Dimensional constants to solve the heat transfer of the fins.

#### 4.2.2 Reynolds number

In this study, the evaluation of Reynolds number is essential to determine the heat transfer rate of the fins. According to Crowe, Reynolds number is a dimensionless number that gives a measure of the ratio of inertial forces to viscous forces [16].

It quantifies the relative importance of these two types of forces for given flow conditions. The formula that is used in this study to evaluate the Reynolds number is:

$$Re_D = \frac{\rho V D_H}{\mu}$$

Where  $\rho$  is the density of the flue gas (kg/m<sup>3</sup>),  
 $V$  is the mean velocity (m/s),  
 $D_H$  is the hydraulic diameter (m), and  
 $\mu$  is the viscosity (kg/m.s).

Assuming that the mass flow rate of the flue gases source is 0.25 kg/s, the mean velocity of the flue gas flow is then 11.73 m/s, acquired using the following equation.

$$\dot{m} = \rho A_C V$$

The Reynolds number evaluated is 14071.82, which falls under a turbulent flow.

### 4.2.3 Frictional factors evaluation

In this study, there are pressure drops in the system which involves the roughness of the surface condition where the fluid flows [11]. A few frictional factor correlations have been developed by a number of mathematicians, and some of them will be compared and considered in this study (table 4.3):

The Colebrook equation requires iterations to be done in order to acquire the values of the frictional factor [19]. The term  $\epsilon/D_H$  relates to the relative roughness of aluminum plate, which  $\epsilon$  can be acquired from the Moody chart in the appendices section. The relative roughness is then calculated to be 0.000483. In this study, we have considered the use of Petukhov's correlation.

Correlation	Formula	Conditions	Values	
Petukhov	$f = (0.790 \ln Re_D - 1.64)^{-2}$	(3000 < Re < 5e6)	0.02867	
Colebrook	$\frac{1}{\sqrt{f}} = -2 \log_{10} \left( \frac{\epsilon/D_h}{3.7} + \frac{2.51}{Re\sqrt{f}} \right)$	(Re > 4000)	1 <sup>st</sup> iteration	0.02912
			2 <sup>nd</sup> iteration	0.02915
			3 <sup>rd</sup> iteration	0.02909
Haaland	$\frac{1}{\sqrt{f}} = -1.8 \log_{10} \left[ \left( \frac{\epsilon/D}{3.7} \right)^{1.11} + \frac{6.9}{Re} \right]$	(Re > 4000)	0.02889	
Swamee Jain	$f = \frac{0.25}{[\log_{10}(\frac{\epsilon}{3.7D} + \frac{5.74}{Re^{0.9}})]^2}$	(5e3 < Re < 1e8)	0.02835	

Table 4.3: Frictional factors correlations.

### 4.2.3 Convection heat transfer coefficient, $h$

The Nusselt's number can be acquired using the following equation provided by Gnielinski [11], which error can be around 10%:

$$\text{Nu}_D = \frac{(f/8)(\text{Re}_D - 1000)\text{Pr}}{1 + 12.7(f/8)^{0.5}(\text{Pr}^{2/3} - 1)} = 40.68$$

The heat coefficient can be calculated via equation after the evaluation of Nusselt's number,  $h$ :

$$h = \frac{\text{Nu}_D K}{D_H} = 23.75 \text{ W/m}^2\text{K}$$

After evaluation of the Nusselt number, the later tables in this section can be generated to have a systematic arrangement of all the data to perform calculations that will yield the heat transfer rate of the gas to gas heat exchanger of the study.

#### 4.2.4 Heat transfer of finned plate.

The attributes of the fins are as follows (table 4.4):

Attributes	Formula/Units	Value
Number of fins	$N$	9
Prime surface, (m <sup>2</sup> )	$A_b$	1.5
Fin width, (m)	$W$	1.5
Fin length (m)	$L$	0.04
Fin thickness (m)	$t$	0.002
Fin cross sectional area (m <sup>2</sup> )	$t \times W = A_c$	0.003
$L_c$ (m)	$L + t / 2$	0.041
$m$	$\sqrt{hP/kA_c}$	654
Surface area of a fin, $A_f$ (m <sup>2</sup> )	$2WL_c$	0.123
Total area, $A_t$ (m <sup>2</sup> )	$A_b + N(A_f)$	2.607
Aluminum thermal conductivity, $k$	(W/m.K)	237

Table 4.4: Fin attributes.

These fins attributes are important and can be varied throughout the design stages to ensure that the final design of the gas to gas finned absorber plate can fit into the design and at the same time achieve maximum efficiency; highest heat transfer rate. Using Microsoft Excel, the parameters can be varied and the characteristic of each absorber plate can be observed.

Some of the temperature attributes are acquired from Seow's analysis [3]. The temperature attributes are as follows (table 4.5):

Attributes	Formula/Units	Value
Inlet flue gas temperature, $T_i$	K	850
Exit flue gas temperature, $T_e$	K	842.91
Mean flue gas temperature, $T_m$	$(T_i + T_e)/2$	846.5
Plate temperature, $T_p$	K	394
Temperature distribution, $\theta_b$	$T_m - T_p$	452.5

Table 4.5: Temperature attributes of fins to calculate heat transfer.

Based on the two tables (table 4.4 and 4.5), the heat transfer of the finned absorber plate can then be determined as follow:

Attributes	Formula/Units	Value
Heat transfer of one fin, $q_f$ (W)	$\sqrt{hPk\theta_b A_c} \tanh mL$	3222.45
Heat transfer without fins, $q$ (W)	$hA_f\theta_b$	1321.70
Efficiency of a fin, $\gamma_f$	$q_f/q$	2.44
Overall fin efficiency, $\gamma_0$	$1 - \frac{NA_f}{A_t} (1 - \gamma_f)$	1.66
Total heat transfer of fins and base, $q_t$ (W)	$h\gamma_0\theta_b A_t$	45120.24

Table 4.6: Finned absorber plate heat transfer.

Three different type of absorber plates are considered in this comparison, which is the finned absorber plate, the corrugated absorber plate and the flat plate. The comparisons are shown as follows, where all the percentage of improvements are calculated relative to the flat plate:

Type of plate	Total area (m <sup>2</sup> )	Heat transfer rate, $q_t$ (W)	Improvement (%)
Finned aluminum plate	2.607	<b>45120.24</b>	<b>179%</b>
Flat plate	1.5	16118.26	-
Corrugated plate	2.357	25321.75	57%

Table 4.7: Comparison of different absorber plates.

From table 4.7, we can see that the heat transfer rate of a finned aluminum plate is proven theoretically to be near twice more efficient than the other absorber plates.

### 4.3 PRESSURE DROP IN NEW CHIMNEY DESIGN

The important parameters for the design of the chimney are the height of the chimney, the inlet and the outlet of the chimney. As mentioned, the main intention of the restricted chimney outlet is to increase the exit velocity and decrease the pressure there, parallel to the principles of Bernoulli equation shown below [16]:

$$z_1 - z_2 = \frac{P_2 - P_1}{\rho \cdot g} + \frac{V_2^2 - V_1^2}{2g} + h_{\text{friction}} + h_{\text{rotor}} + h_{\text{minor}}$$

The equation clearly suggests that the pressure drop in the chimney will increase as the height, H increases. Hence, there will be a higher pressure drop to create higher driving force on the circular wind rotor.

The change of pressure for the chimney and the inlet and exit velocities (conservation of mass flow rate equation) can be calculated via the equations below:

$$\Delta P = \rho \cdot g \cdot \Delta H$$

$$\rho \cdot A_i \cdot V_i = \rho \cdot A_e \cdot V_e$$

$$V_{\text{avg}} = (V_i + V_e)/2$$

Where  $\Delta P$  is the change of pressure due to the elevation,  $\rho$  is the density of air,  $g$  is the gravitational acceleration and  $H$  is the elevation change. The summary of the parameters to calculate the pressure drop is as follows, assuming a mass flow rate of 0.25 kg/s:

Factors	Temp (C)	Air density (kg/m <sup>3</sup> )	Air velocity (m/s)	Area equation	Area (m <sup>2</sup> )
Body inlet	20	1.208	1.29	1m x 0.05m	0.05
Chimney outlet	26.2	1.183	20.85	$\pi(0.076^2) - \pi(0.051^2)$	0.0101
Mean	23.1	1.195	11.07	-	-

Table 4.8: Table of summary of design parameters for pressure drop.

Using the following equations below, the head losses (rotor, friction and minor) are considered as the pressure drop in the chimney is calculated.

$$h_{\text{rotor}} = C_p \cdot \left( \frac{V_{\text{avg}}^2}{2 \cdot g} \right)$$

$$h_{\text{friction}} = \sum f \left( \frac{L}{D} \right) \cdot \left( \frac{V_{\text{avg}}^2}{2 \cdot g} \right)$$

$$h_{\text{minor}} = \sum K_c \left( \frac{V_{\text{avg}}^2}{2 \cdot g} \right)$$

The value of Reynold's number is 14073, and thus is a turbulent flow and the value of friction factor,  $f$  is determined using the Petukhov equation ( $3000 < Re < 5e6$ ) after evaluating the  $Re$  and has a value of 0.0265.

In order to calculate the friction head loss, the system is divided into two; the body and also the chimney. Both the head losses are obtained and summed.

For the minor head losses, there are 4 changes in shape factors; 2 constrictions with  $K_c$  values of 0.04 and 2 elbows with  $K_c$  values of 0.4.  $C_p$  is the power coefficient for the circular wind rotor in a closed conduit, in which analytically, has an average value of 0.6. The calculated values (manipulating the mass flow rate) are as per table below:

$M_{\text{flue}}$ (kg/s)	Friction factor, $f$	Frictional loss (m)	Minor Loss (m)	Rotor loss (m)	Pressure drop (Pa)
0.10	0.0184	0.1712	1.0836	0.2128	81.70
0.25	0.0153	0.8871	6.7727	3.3245	415.32
0.50	0.0134	3.1128	27.0908	26.5961	1749.24

Table 4.9: Tabulated results of pressure drop at different mass flow rates.

4.4 CAD MODELLING

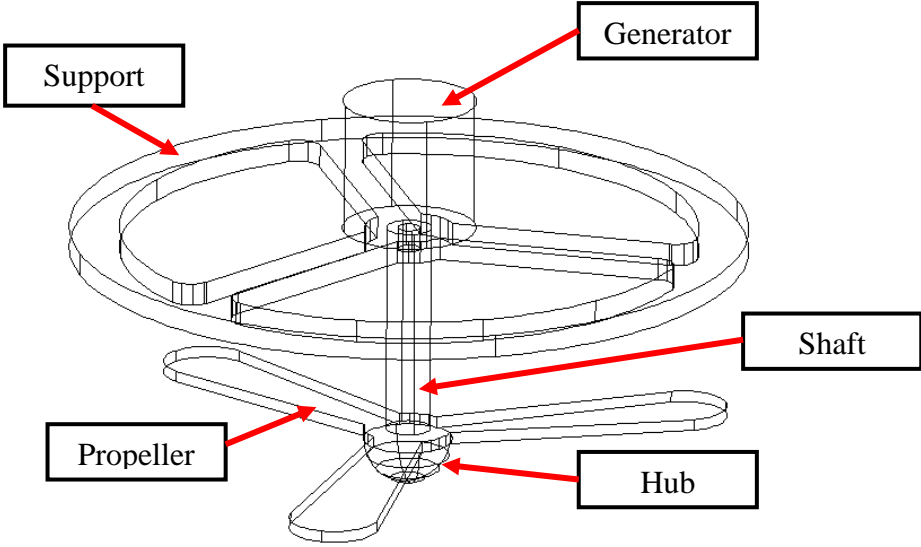


Figure 4.11: Generator assembly.

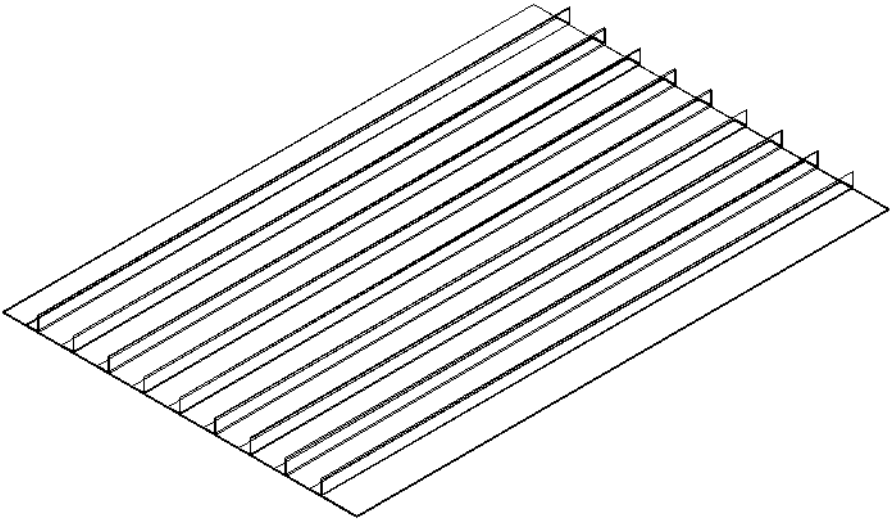


Figure 4.12: ISO view of the finned aluminum absorber plate.

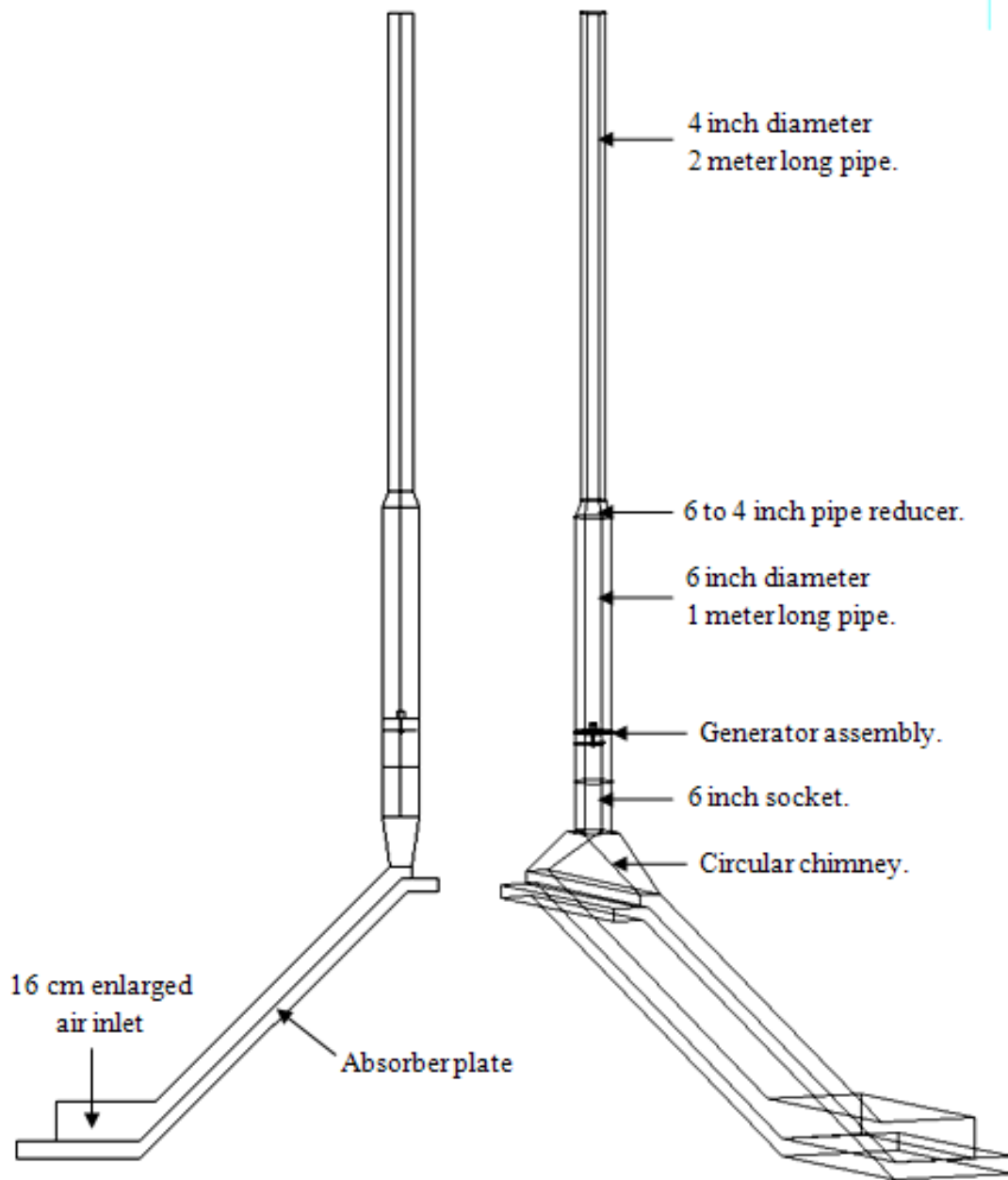


Figure 4.13: Completed model.

## CHAPTER 5

### EXPERIMENTAL DATA

In this section, the experimental results are shown for tests run on the flue gas mode, the solar mode and also the hybrid mode. Besides that, some of the problems that occurred are also highlighted in the following section followed by recommendations for project enhancement.

#### 5.1 EXPERIMENT SETUP

##### 5.1.1 Instrumentation

Instrumentations are used to measure some of the essential data that are required in experiments. In this study, some of the instruments that are used to measure variables are tabulated in table 5.1:

Label	Variable	Instrument
Figure 5.1	Angular velocity.	Digital Tachometer.
Figure 5.2	Absorber plate temperature.	Infrared Thermometer.
Figure 5.3	Rotor torque.	Drill like Torque-meter.
Figure 5.4	Air inlet and outlet velocity and temperature.	Digital Anemometer.
Figure 5.5	Solar intensity	Light/Solari meter

Table 5.1: Instrumentations to measure data for experiment.



Figure 5.1: Digital tachometer.



Figure 5.2: Infrared thermometer.



Figure 5.3: Torque meter.



Figure 5.4: Digital hot wire anemometer.



Figure 5.5: Light/Solari Meter.

As mentioned, due to the insufficient updraft air velocity, several variables were deprived and as a result, the torque meter and the digital tachometer were not used in the experiment.

### 5.1.2 Data acquisition

Figure 5.6 below shows the schematic diagrams of points where data will be acquired and tabulated. T refers to temperature and will be measured by the digital hot wire anemometer at  $T_{\text{air.out}}$  and  $T_{\text{air.in}}$  while  $T_{\text{plate.out}}$  and  $T_{\text{plate.in}}$  will be measured with the infrared thermometer.  $V_{\text{in}}$ ,  $V_{\text{out.1}}$  and  $V_{\text{out.2}}$  will be measured using the digital tachometer.

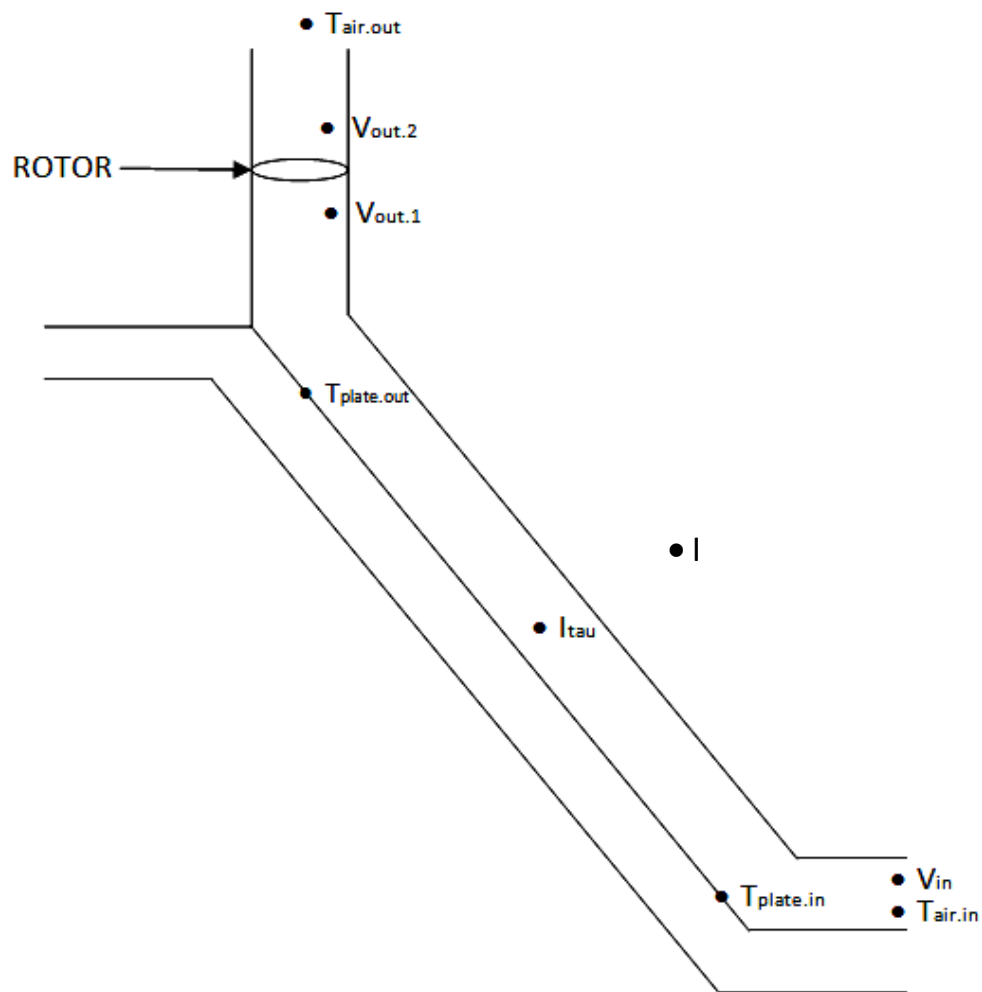


Figure 5.6: Schematic diagram of measurement points.

## 5.2 EXPERIMENTS CONDUCTED

Three sets of experiments were conducted as proposed in the objective of this study; using the flue gas mode, the solar mode and lastly the hybrid mode (combination of the flue gas mode and solar mode)

### 5.2.1 Flue Gas Mode

A trial experiment was conducted after the gas turbine, connections between the hybrid solar chimney and safety equipments such as emergency doors and fire extinguishers are prepared. The gas turbine was started with compressed air for 10 minutes where at that point of time; the model was checked for air leaks and was modified as shown in section 5.3.1.



Figure 5.7: The technician firing up the gas turbine.

As the lab technician fired up the gas turbine, a flue gas temperature of around 600°C (873 K) was achieved. There were a few limitations using the gas turbine:

- i. If the temperature of the combustion drops to achieve the limited flue gas temperature (lower than 600°C), the gas turbine will automatically shut down its operation.
- ii. The gas turbine cannot be operated for a long period of time (a safe zone of 20 minutes) due to limitations of the compressors cooling mechanism.

As the test run with flue gas temperature of 600°C was run, after around 5 minutes, there was smoke coming out of the flue gas passage of the hybrid model. The operation was stopped and the model was modified again. This design problem is highlighted in section 5.3.2.

After the modification, the experiment was conducted again. The same procedures were followed and the following results were acquired in the table below. As mentioned, the experiment was conducted for 20 minutes with an average flue gas temperature of 850K.

Properties / Interval (mins)		0	10	20
Air temperature	Tair.in (K)	24.4	40.2	42.6
	Tair.out (K)	24.7	53.5	58.6
Absorber plate temperature	Tplate.in (K)	23.3	190.3	214.1
	Tplate.out (K)	22.4	160.5	182.5
Velocity of air	Vin (m/s)	0	0.1	0.2
	Vout.1 (m/s)	0	0.4	0.7
	Vout.2 (m/s)	0	0.5	0.8

Table 5.2: Results for flue gas mode.

## 5.2.2 Solar Mode

Before the experiment was conducted, a few basic configurations of the solar model related to the sun must be noted:

- i. Latitude and longitude of the experiment site.
- ii. Model orientation (compass).
- iii. Weather forecast.
- iv. Local time forecast for sunrise and sunset.
- v. The flue gas passage must be blocked to avoid unnecessary heat lost.

In this study, the experiment is conducted in Tronoh, Malaysia which has latitude of 4.417 degrees ( $4^{\circ} 25' 1''$ ) North of the Equator and longitude of 100.983 degrees ( $100^{\circ} 58' 58''$ ) East of the Prime Meridian on the world map.

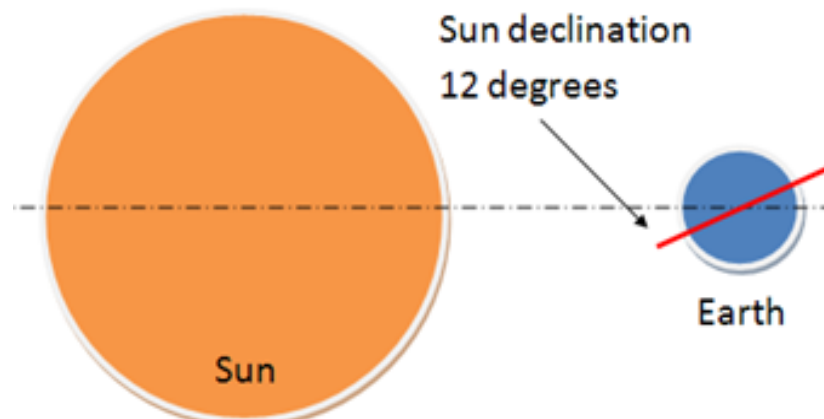


Figure 5.8: Declination of sun.

The orientation of the model depends highly on coordinate of the model in the globe and also the timing of the experiment. The solar mode experiment was performed in the month of August and the model is proposed to face to the south to avoid shadowing by the tall chimney.

A solar calculator was used in the analysis of acquiring the declination of the sun and the declination of the sun on the day of experiment (21<sup>st</sup> August 2009) was a positive 12 degrees.

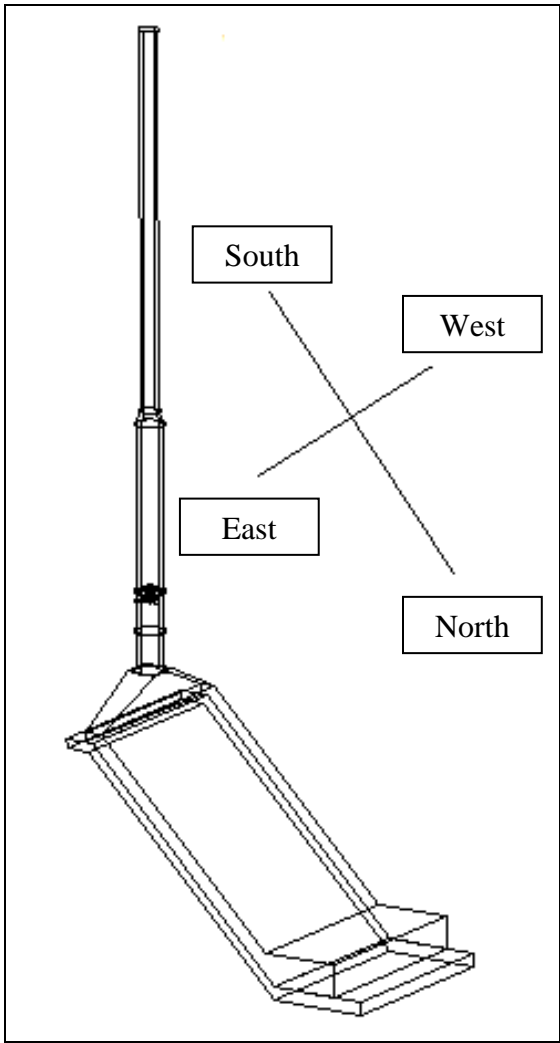


Figure 5.9: Orientation of the hybrid solar chimney model.

Date: 21/8/09

Weather: Cloudy after rain in the morning.

Properties / Time		9am	10am	11am	12pm	1pm	2pm	3pm	4pm
Air temperature (°C)	Tair.in	26.5	27.9	34.4	34.8	36.2	38.5	35.6	31.2
	Tair.out	27.4	28.3	35.7	38.1	40.2	40.5	38.8	34.9
Absorber plate temperature (°C)	Tplate.in	35.6	36.9	47.4	54.1	55.9	61.1	61.0	54.5
	Tplate.out	31.7	33.9	42.3	49.1	50.3	52.7	54.5	50.5
Velocity of air (m/s)	Vin	0.0	0.0	0.0	0.0	0.0	0.0	0.0	0.0
	Vout.1	0.0	0.0	0.0	0.0	0.1	0.1	0.1	0.1
	Vout.2	0.0	0.0	0.0	0.0	0.1	0.1	0.1	0.1
I (W/m <sup>2</sup> )		91.5	133.0	287.0	531.4	608.8	592.0	562.2	233.5
Itau (W/m <sup>2</sup> )		41.3	86.3	142.2	279.0	385.0	378.3	377.8	93.5

Table 5.3: Solar mode results.

More experiments are to be conducted in the future to obtain more data for the solar mode.



Figure 5.10: Usage of compass to check the orientation.

### 5.2.3 Hybrid Mode

In the hybrid mode experiment, the gas turbine is not used because the gas turbine mechanism is not mobile and is almost permanent in the lab. Thus another alternative is to propose another burner mechanism that can produce a flue gas with a temperature of around more than 100 degrees Celsius.

The burner that was proposed is a lab scaled waste incinerator (figure 5.11). Previous experiments conducted using dried branches and leaves as fuel yielded a flue gas temperature of around 200 degrees Celsius.



Figure 5.11: Lab scaled incinerator used for hybrid mode experiments.

Charcoal (figure 5.12) was used as an alternative fuel source due to its long lasting burning effect. The flue gas supply must be constant from 9am until 4pm to ensure that the experiments are simulated in an ideal environment. The flue gas temperature that is yielded from using charcoal is around 100 degrees Celsius.



Figure 5.12: Alternative fuel for lab scaled incinerator, charcoal.

All the necessary preparations are done accordingly for the solar mode as mentioned in section 5.2.2; angle of declination, instrumentations and others. The flue gas inlet is connected to the flue gas outlet of the incinerator as shown in figure 5.11.

The incinerator is functional before 9am to ensure constant flue gas temperature throughout the experiment period.

Table 5.4 shows the data that is acquired from this hybrid mode experiment.

Date: 16 September 2009

Weather: Cloudy morning

Properties / Time		9am	10am	11am	12pm	1pm	2pm	3pm	4pm
Air temperature (°C)	$T_{air.in}$	34.5	34.7	34.8	35.3	37.3	40.4	39.3	37.7
	$T_{air.out}$	34.9	34.8	35.8	36.5	40.5	42.4	41.2	40.2
Absorber plate temperature (°C)	$T_{plate.in}$	39.5	44.9	55.2	57.3	60.1	66.1	60.3	58.3
	$T_{plate.out}$	38.0	39.2	51.7	54.6	56.3	60.5	54.2	54.6
Velocity of air (m/s)	$V_{in}$	0.0	0.0	0.0	0.0	0.0	0.1	0.0	0.0
	$V_{out.1}$	0.0	0.0	0.0	0.0	0.1	0.2	0.1	0.0
	$V_{out.2}$	0.0	0.0	0.0	0.1	0.2	0.3	0.1	0.1
$I$ (W/m <sup>2</sup> )		219.4	359.9	447.6	563.6	584.6	600.3	565.4	461.5
$I_{tau}$ (W/m <sup>2</sup> )		124.5	192.7	285.1	322.3	343.0	350.6	332.6	295.2
Flue temperature (°C)	$T_{air.in}$	54.6	77	102.1	104.3	100.3	96.4	89.1	84.6
	$T_{air.out}$	35	35.6	36.5	36.6	40.1	42.3	41.3	39.6

Table 5.4: Tabulated hybrid mode results.

## 5.3 DESIGN PROBLEMS

### 5.3.1 Air leakage test

An air leak was identified as per pictures below during the test run:

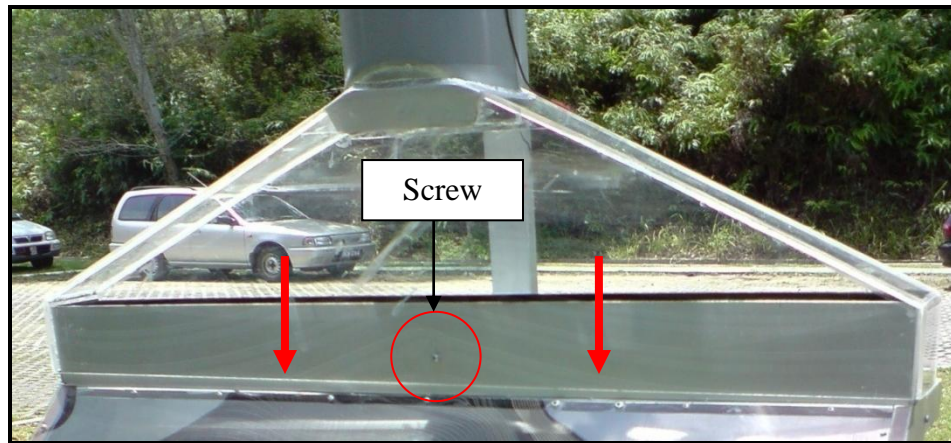


Figure 5.13: Air movement out of chimney slot.

As a result, the chimney slot was simply fastened to the model with a screw to prevent air from exiting (Figure 5.13). The escaped air will caused significant decrease in efficiency.

### 5.3.2 Flue gas impingement

There was initially 1 layer of asbestos at the point of direct hot flue gas impingement and it was enforced with another layer of it when modified. The model was redesigned by putting a thick aluminum layer at the point of direct flue gas impingement covered by

a large stainless steel deflector plate (figure 5.17) to overlap the gap created by the 45 degrees tilt.

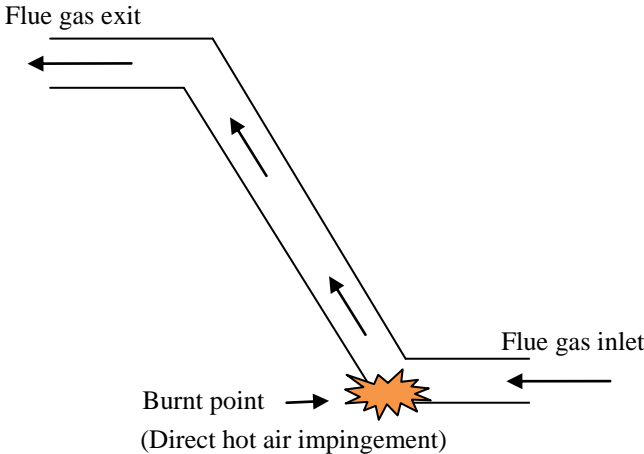


Figure 5.13: Air movement out of chimney slot.



Figure 5.15: Burnt asbestos due to direct flue gas impingement.



Figure 5.16: Installation of a stainless steel deflector plate to overlap tilt gap.

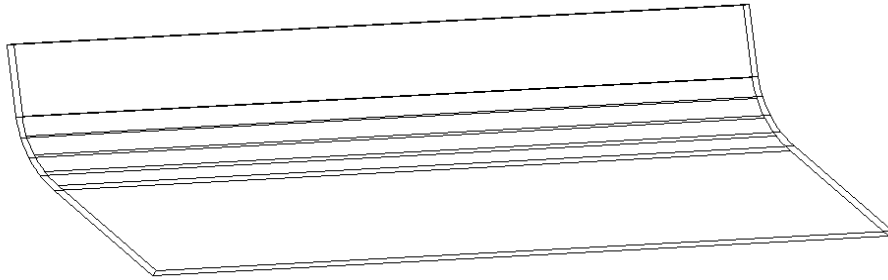


Figure 5.17: Stainless steel deflector plate shape.

### 5.3.3 Diffuser design

The current diffuser design is according to figure 5.18. The flue gas inlet pipe is protruding inside, leading the flue gas to directly impinge the asbestos layer at the tilted gap without being diffused. In other words, the hot flue gas will be in contact with only the middle of the absorber plate all the way out to the exit. There will be no heat distribution in the passage.



Figure 5.18: The flue gas diffuser (inlet).



Figure 5.19: Current diffuser design.

The diffuser should be designed to include splitting vanes and simulated in FLUENT or GAMBIT to acquire a rough idea of its capabilities of diffusing the flue gases.

## **CHAPTER 6**

### **DATA ANALYSIS**

In this chapter, the data acquired from performing the 3 experiments; hybrid mode, solar mode and flue gas mode is analyzed accordingly.

#### **6.1 FLUE GAS MODE**

The results of the flue gas mode can be seen in table 5.2. As can be observed, the maximum velocity of updraft air is 0.8 m/s, which is very encouraging result for a lab scaled hybrid solar chimney.

This model can be scaled up to a desired size to acquire a desirable updraft air velocity to acquire sufficient energy to propel the wind rotor and generate power. A velocity of at 3 m/s is required to acquire propulsion of the wind rotor.

If the gas turbine is able to provide constant flue gas for a longer period of time, the study can be more elaborated and this study will be able to mimic the ideal environment where the hybrid solar chimney is installed in the power plants in the future.

From the limited 20 minutes experiment, the maximum air temperature difference is a massive 16 degrees Celsius, while the maximum absorber plate temperature difference is 31.6 degrees Celsius. These temperature differences are very significant and show that the hybrid solar chimney is viable to be developed for commercial use.

The two graphs (figure 6.1 and 6.2) show how the temperature differences of the updraft air at inlet and outlet and the absorber plate temperature in and out differences compared to the maximum velocity attained.

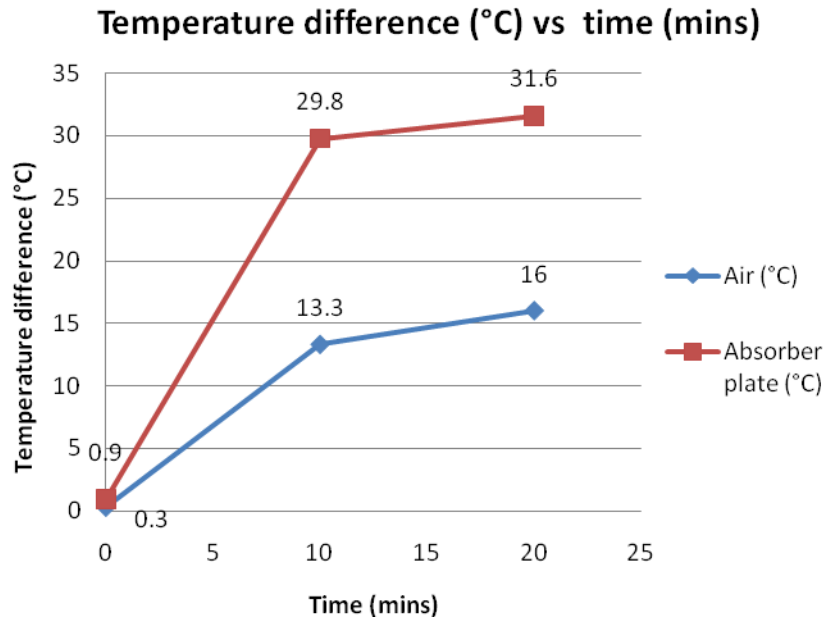


Figure 6.1: Air passage and absorber plate temperature difference vs. time graph.

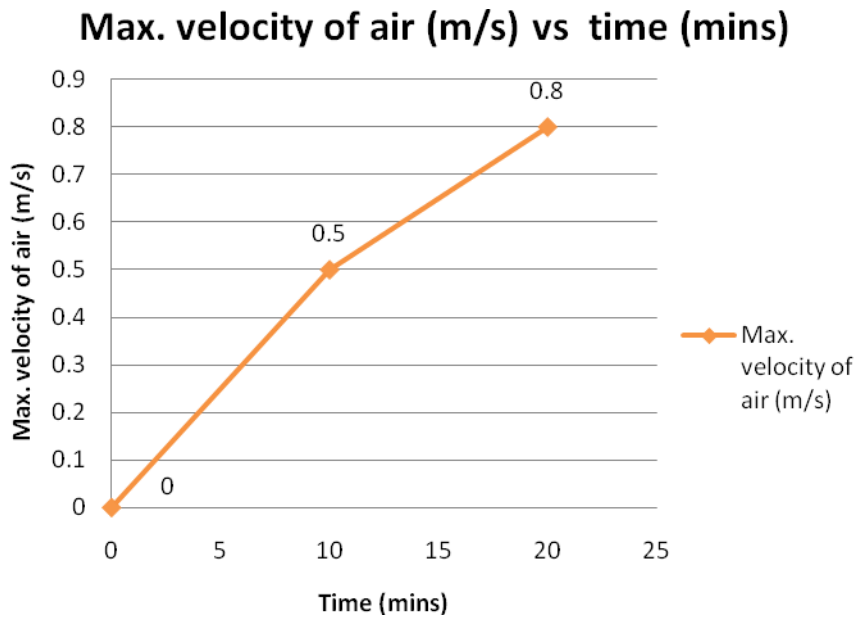


Figure 6.2: Maximum velocity of air vs. time graph.

## 6.2 SOLAR MODE

In the solar mode, after all the precautions discussed in the previous chapter were taken, the results were acquired and tabulated in table 5.3. As can be analyzed in figure 6.3, it is noticed that there is a massive loss of solar radiation, which is directly proportional to thermal energy emitted to the absorber plate, after the solar energy gets filtered by the 4mm thick Perspex. An average of **29%** of solar radiation loss was accounted for throughout the 8 hours (9am til 4pm) experiment due to the 4mm thick Perspex.

The maximum updraft air velocity achieved in this experiment is 0.1 m/s. It is indeed insignificant but in this case, only a lab scaled model is used. By scaling up model significantly (increasing the absorber plate area, air inlet and the other likes), a higher updraft air velocity will be achieved.

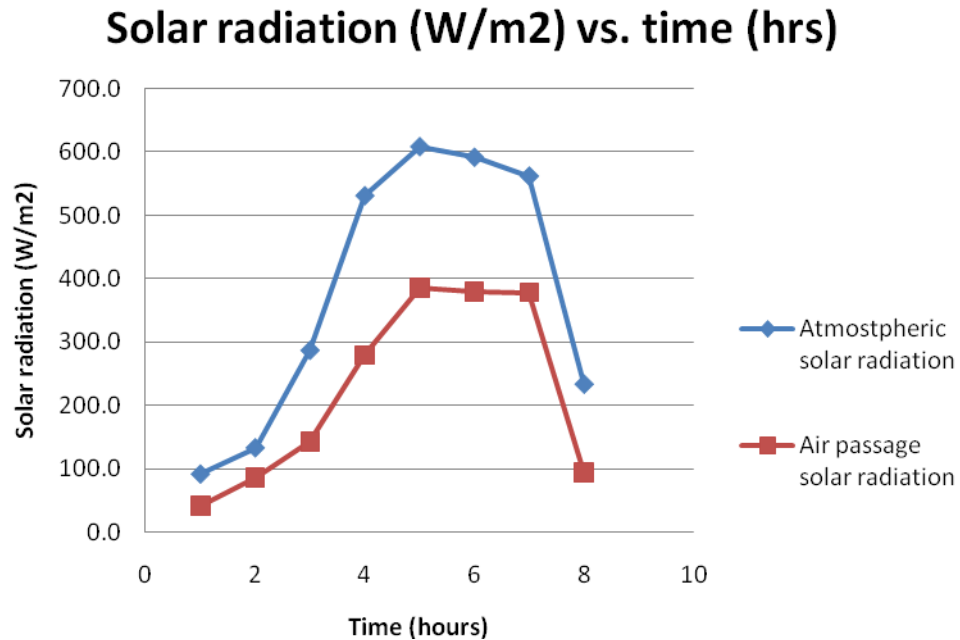


Figure 6.3: Atmospheric solar radiation and solar radiation in air passage.

Considering the solar energy that is manipulated is a free source, a positive end result will always be yielded. The only concern is to increase the efficiency of manipulating the solar thermal energy as efficient as possible in order to generate more electricity from the system.

### **6.3 HYBRID AND SOLAR COMPARISON**

The two modes (solar and hybrid) are compared to see the efficiency of the entire system. As mentioned, the flue gas in the hybrid mode is produced by a lab scaled incinerator which produces a flue gas temperature of around 100 degrees Celsius constantly throughout the experiment period.

By combining a flue gas source of around 100 degrees Celsius to the solar mode to become the supposedly hybrid solar chimney, the efficiency of the system increased by almost 10%.

This is proven by calculating the temperature difference of the updraft air (out minus in) and the absorber plate (in minus out) and getting the average percentage of increase. The average percentage of temperature difference between the outlet and inlet of the absorber plate is **9.6%** improved. The average percentage of the temperature difference between the inlet and outlet of the updraft air is **9.2%** improved.

When the temperature difference between the inlet and outlet of the absorber plate is high, transfer of thermal energy to the air passage is high and that will result in higher velocity of updraft air. High temperature differences of the updraft air in the inlet and outlet proves that heat inside the flue gas passage and thermal energy from solar radiation is effectively used to heat the air in the air passage.

Time		9am	10am	11am	12pm	1pm	2pm	3pm	4pm	
Maximum velocity of updraft air (m/s)	Hybrid	0.0	0.0	0.0	0.1	0.2	0.3	0.1	0.1	
	Solar	0.0	0.0	0.0	0.0	0.1	0.1	0.1	0.1	
Absorber plate temperature (°C)	Hybrid	out	39.5	44.9	55.2	57.3	60.1	66.1	60.3	58.3
		in	38.0	39.2	51.7	54.6	56.3	60.5	54.2	54.6
	Solar	out	35.6	36.9	47.4	54.1	55.9	61.1	61.0	54.5
		in	31.7	33.9	42.3	49.1	50.3	52.7	54.5	50.5
Air temperature (°C)	Hybrid	out	34.9	34.8	35.8	36.5	40.5	42.4	41.2	40.2
		in	34.5	34.7	34.8	35.3	37.3	40.4	39.3	37.7
	Solar	out	27.4	28.3	35.7	38.1	40.2	40.5	38.8	34.9
		in	26.5	27.9	34.4	34.8	36.2	38.5	35.6	31.2
Flue temperature for hybrid mode (°C)	Tair.in	54.6	77	102.1	104.3	100.3	96.4	89.1	84.6	
	Tair.out	35	35.6	36.5	36.6	40.1	42.3	41.3	39.6	

Table 6.1: Comparison between hybrid mode and solar mode.

The graphs (figure 6.4, 6.5, 6.6, and 6.7) show the absorber plate and air passage comparisons between the hybrid mode and also the solar mode.

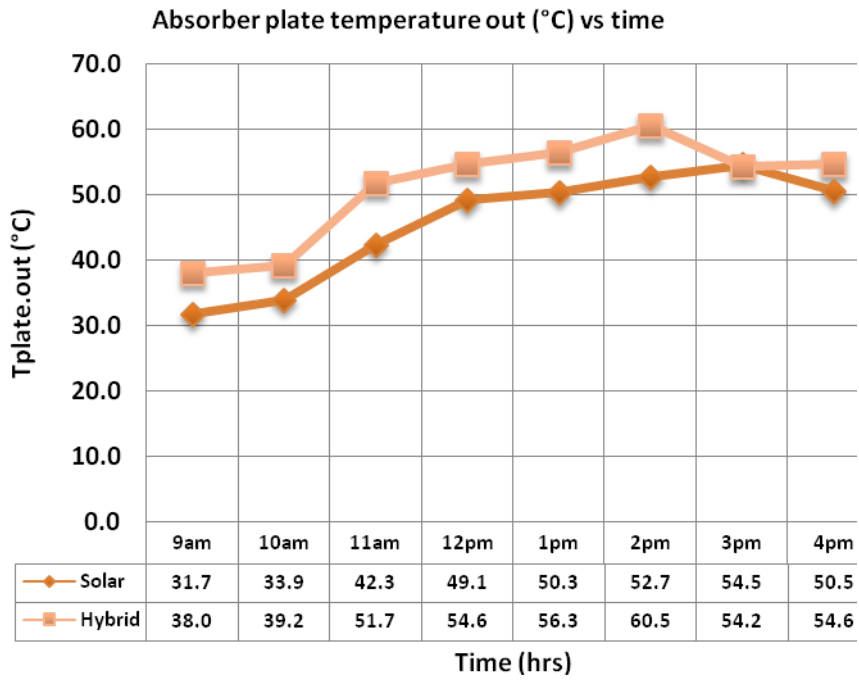


Figure 6.4: Absorber plate temperature out (°C) vs. time graph.

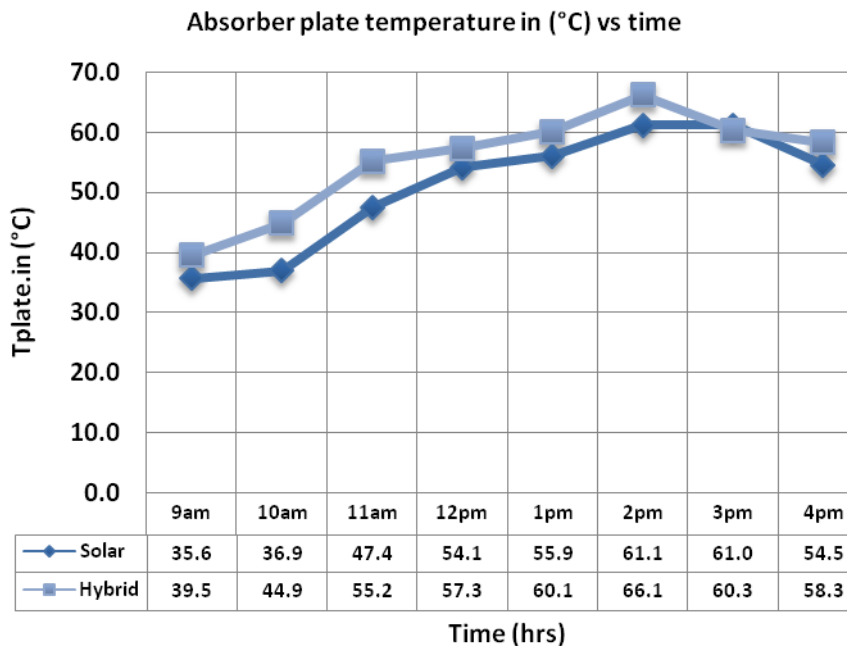


Figure 6.5: Absorber plate temperature in (°C) vs. time graph.

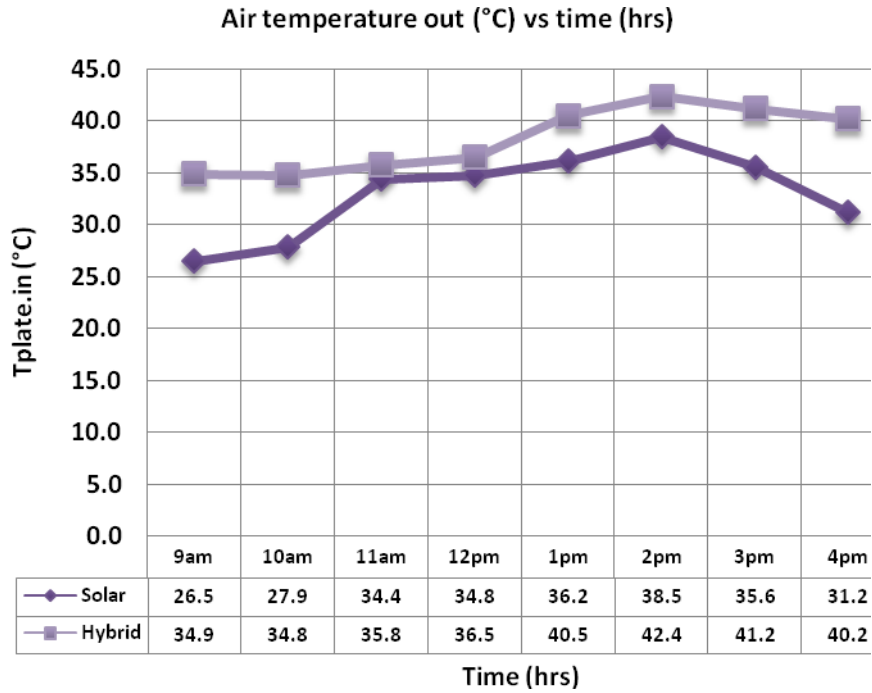


Figure 6.6: Air temperature out (°C) vs time (hrs) graph.

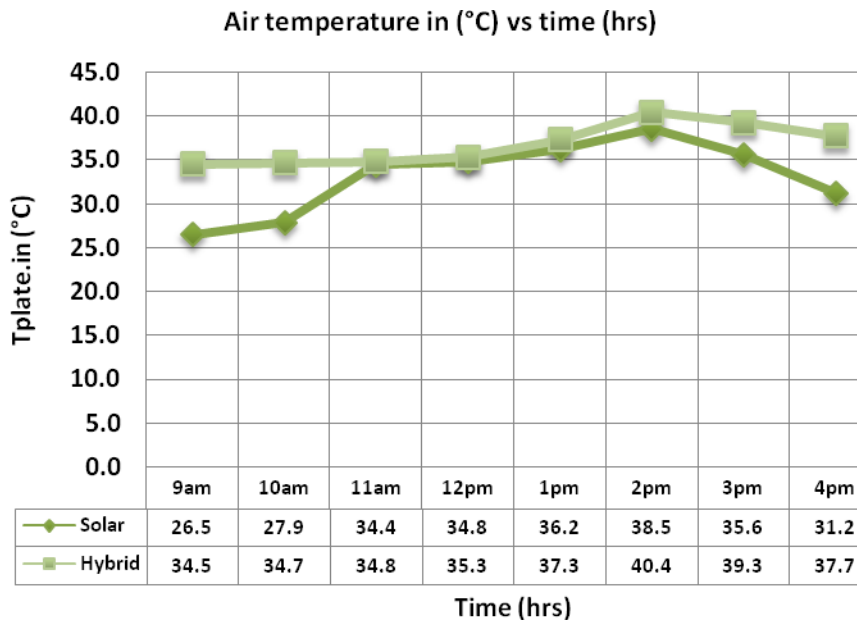


Figure 6.7: Air temperature in (°C) vs time (hrs)

## CHAPTER 7

### RECOMMENDATIONS

In this section, some of the possible ideas and thoughts that are driven towards enhancing the hybrid solar chimney is listed and discussed.

#### 7.1 ENHANCEMENTS.

Some enhancements can be done in the future to the hybrid model in order to acquire higher efficiency and better results. The recommendations are listed as follows:

##### 7.1.1 Physical designs

- i. Splitting vanes are used in the diffuser to distribute the flue gas effectively to be in contact with the whole absorber plate. Simulation works can be done to acquire higher efficiency in diffusing the flue gas effectively (Figure 7.1).

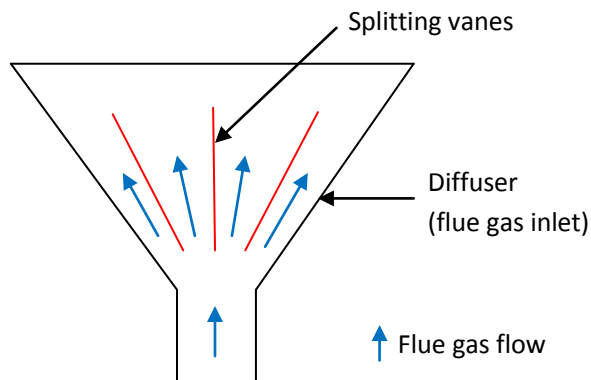


Figure 7.1: Splitting vanes on diffuser.

- ii. Sharp ends at flue gas or air passage should be avoided to ensure undisturbed fluid flow and avoid circulation (Figure 7.2).

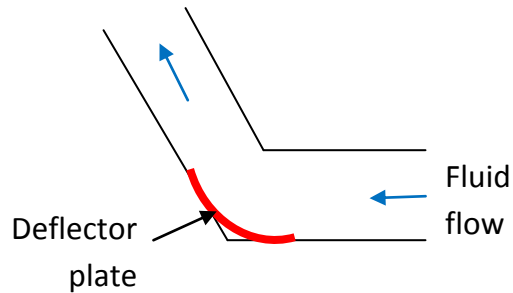


Figure 7.2: Deflector plate.

- iii. A better material selection; wood should be avoided in high temperature appliances to avoid fire accidents and Perspex should be changed to glass to avoid changed properties due to high temperature application (Figure 7.3).



Figure 7.3: Wood to be avoided in high temperature experiments.

- iv. A combustor or a machine that will generate constant (at least 1 hour) flue gas at manipulated flow rates and temperatures is used to test the hybrid model in the flue gas mode.
- v. A highly precise symmetrical propeller is fabricated and used to acquire better propulsion by the induced air in the chimney.
- vi. A taller chimney is proposed to acquire higher pressure difference that acts as a driving force for updraft air.
- vii. The absorber plate surface that will be exposed to the sun can be corrugated shape that will avoid shadowing effect and at the same time increase the surface area of the absorber plate to absorb solar thermal energy. Indirectly helps with flue gas distribution and still promote easy fins installation. (Figure 7.4)



Figure 7.4: Corrugated plate with fins used.

- viii. The sensors used are to be calibrated regularly to ensure accuracy of measurement; lightmeter, hot wire anemometer, and infrared thermometer.

- ix. The absorber plate is warmed before the solar experiment is conducted in the morning to ensure that the dews are completely vaporized.
- x. Heat radiation should be taken into consideration in the model's horizontal air and flue gas passage inlet (Figure 7.5).

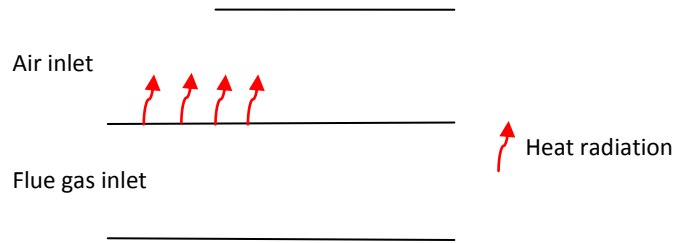


Figure 7.5: Heat radiation from flue gas inlet to air inlet.

- xi. The change in area of the air passage must be minimized. The current design consists of a variety of change of area; the air passage inlet, the chimney slot, the 6 inch circular chimney, and the 4 inch circular chimney. A smaller chimney circular area is proposed to be used to increase the efficiency of the system.
- xii. The rain cover of the model can be modified to become a nozzle to produce a jet of air out when the updraft air is exiting the model. Caution to recirculation and back pressure if implemented.

### 7.1.2 Design concepts

- i. The flue gas passage exit is proposed to be connected to the air passage exit as shown in figure 7.6. This method will work as regeneration as the hot air from the flue gas passage will encourage the flow (velocity) of the updraft air due to buoyancy differences between hot air and cold air.

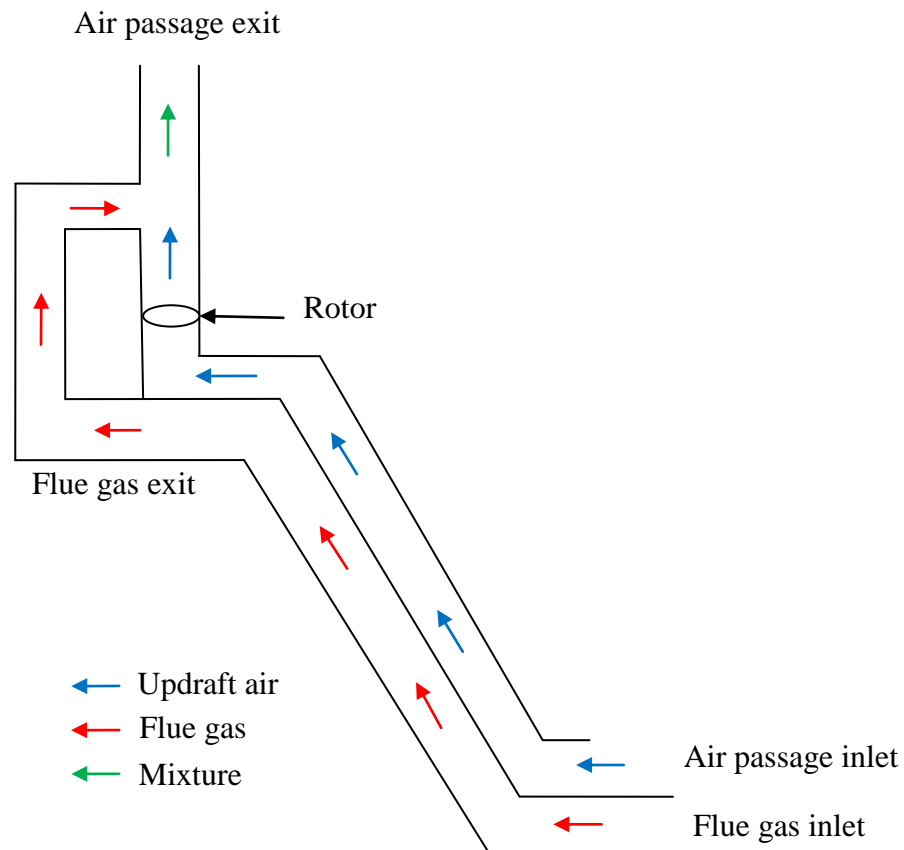


Figure 7.6: Connecting flue gas passage exit to air passage exit.

- ii. The incline of the entire model is proposed to be as shown in figure 7.7. In this figure, as obviously shown, the model's passages are divided into 2, one with a 10 degrees tilt and another with a 45 degrees tilt.

The 10 degrees tilt is essential to 'capture' better solar radiation, in Malaysia. The 10 degrees tilt as well can cause the hot flue gases to stay idle longer in the flue gas passage to encourage more heat transfer to the air passage. This is because hot air particles tend to move up to the absorber plate.

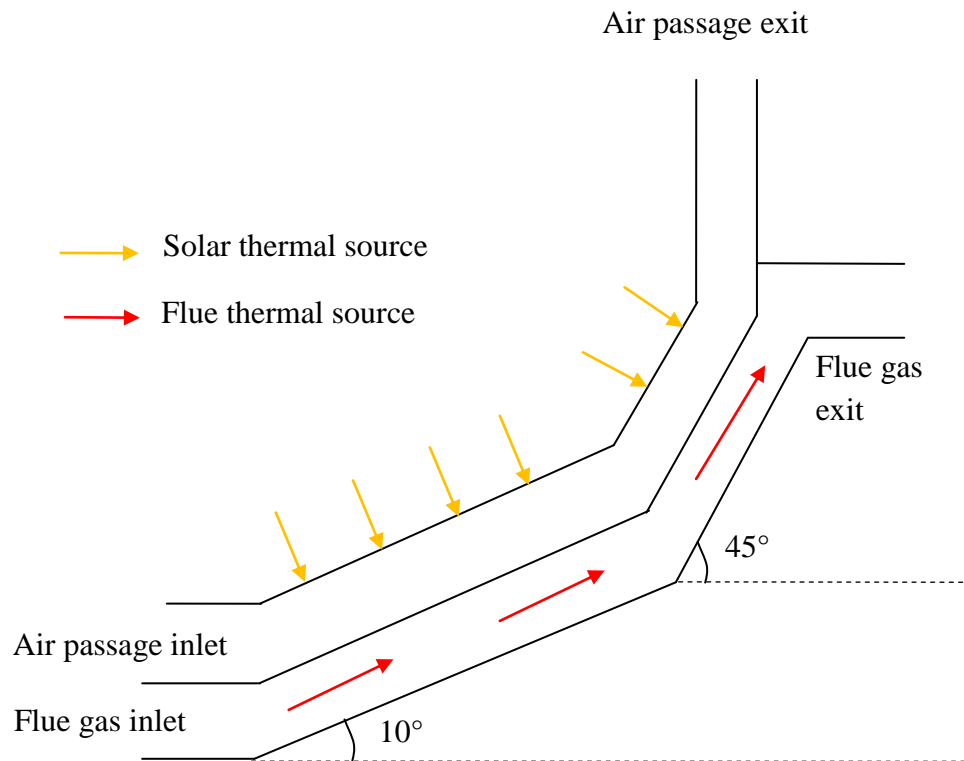


Figure 7.7: New radical proposal of hybrid solar chimney body.

- iii. Ribs can be installed on the base of the flue gas passage and also the fins in the flue gas passage. The ribs, also known as turbulators are used to induce turbulence flow more effectively. Inducing turbulence flow in the flue gas passage and/or air passage will increase the Nusselt number and increase heat transfer. Besides that, the ribs too are used to break laminar sub layers of flow inside the flue gas passage and air passage. The concept of turbulators can be seen in figure 7.8.

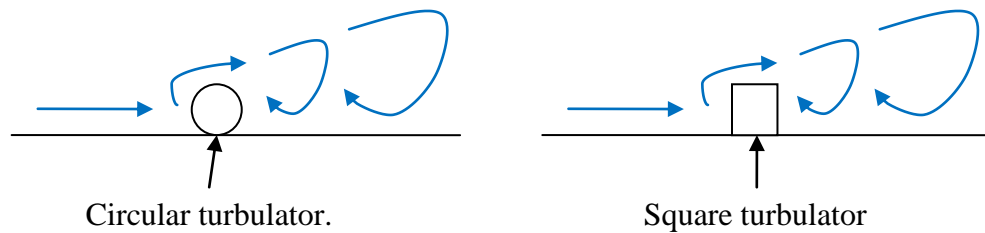


Figure 7.8: Turbulators or ribs concept.

- iv. The velocity profile of the updraft air in the chimney should be more thoroughly analyzed as the current velocity profile is not fully developed when the updraft air comes into contact with the propeller (Figure 7.9).

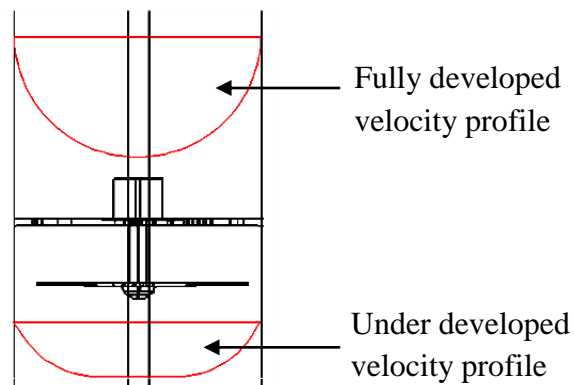


Figure 7.9: Velocity profile diagram for easy understanding.

## **CHAPTER 8**

### **CONCLUSION**

In conclusion, after all the simulations and modifications are done to improve the efficiency of the system; circular chimney, chimney height extension, circular wind rotor, increased air inlet size, absorber plate painted black to name a few, the study shows that combining the solar and flue gas operations together will yield an increased efficiency by almost 10% compared to the solar mode alone.

The flue gas mode was tested using the gas turbine which produced a relatively high flue gas temperature of 600 degrees Celsius. The maximum updraft air velocity induced was 0.8 m/s which are considered very high in this lab scaled model. The solar chimney in reality for commercial power generation covers a diameter of up to 2km, producing only around 5 m/s of induced air velocity.

The objectives of this study have been met successfully and a series of recommendations which covers the physical model improvement of the current hybrid solar chimney and also a few new design concepts are proposed in the later sections of this report. The recommendations are all driven to further improve the efficiency of the development of this hybrid solar chimney.

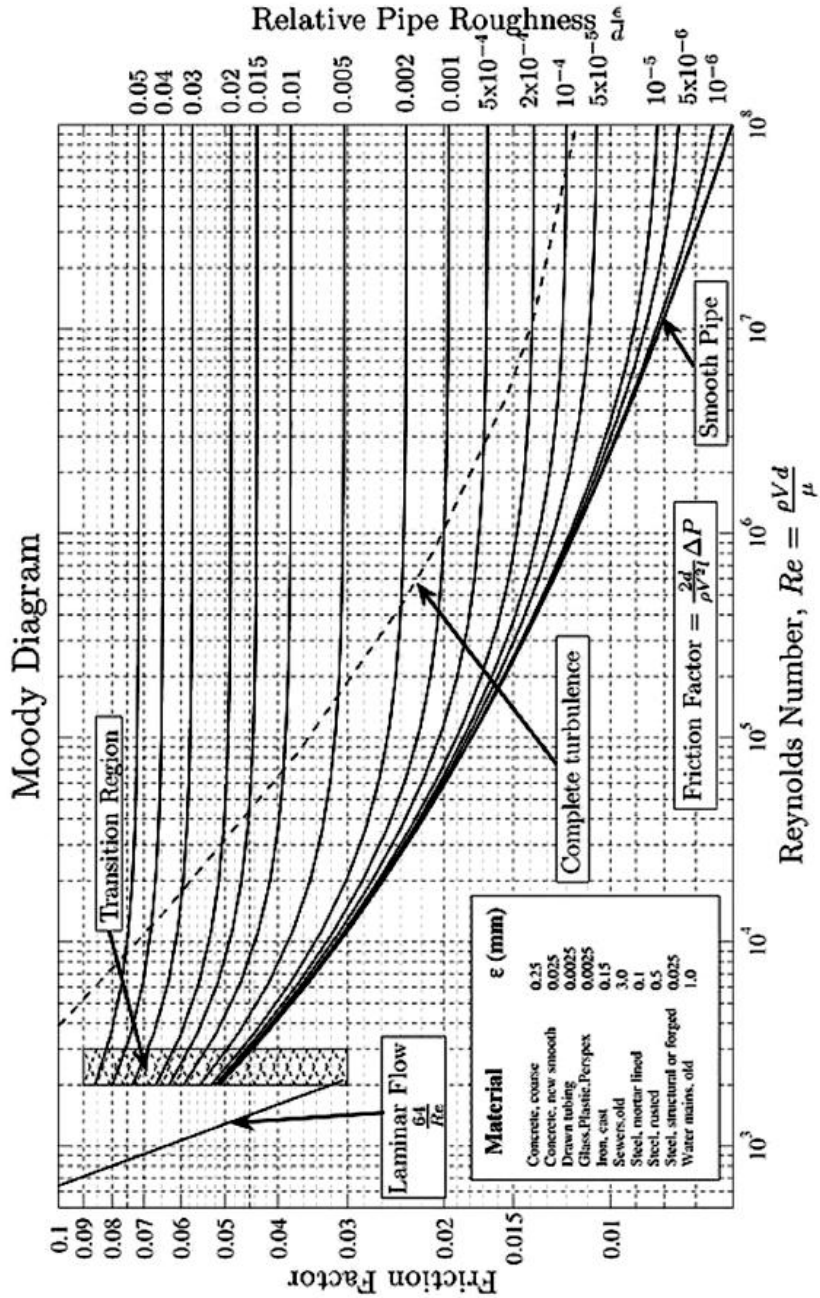
## REFERENCES

- [1] Al-Kayiem, H. H. & Sa'ad Al-Deen, A. E., Performance Analysis of Savonius Wind Rotor for Directed Flow Operation. Proceedings of 1st Engineering Conference on Energy & Environment (EnCon), December 27-28, Kuching, Sarawak, Malaysia, 2007.
- [2] John, 2008, <http://www.alterenergy.co.nz/pg5.html>
- [3] L. L. Seow, 2008, Energy Recovery by Conversion of Thermal Energy of Flue Gases to Electricity, Universiti Teknologi PETRONAS Final Year Project.
- [4] M. S. Balbir, S. Fauziah, 2000, Influence Of Some Parameters On The Efficiency Of A Solar Collector, Platform, Vol 1 No 2, UTP.
- [5] Arvid B, April 2009, Utilization of waste heat, <[www.abco.dk/heatrec.htm](http://www.abco.dk/heatrec.htm)>.
- [6] Phubalan K, 2004, Waste heat recovery in Genting Sanyen, MEPA news, 003.
- [7] Sadik Kakaç and Hongtan Liu (2002). Heat Exchangers: Selection, Rating and Thermal Design (2nd Edition ed.). CRC Press. ISBN 0849309026.
- [8] DKL Engineering, April 2009, <<http://www.sulphuric-acid.com>>
- [9] Alan W, November 2007, The Solar Nozzle, A possible approach for efficient, large scale, Solar electricity.
- [10] Wang J. et al, 1999, The performance of a new gas to gas heat exchanger with strip fin, Energy conversion and management journal, ISSN : 0196-8904
- [11] Incropera et al, 2007, Introduction to heat transfer, 5th edition, John Wiley and Sons Publishing, ISBN 0-471-79472-4
- [12] Washington State University Energy Program, <[www.flasolar.com/active\\_dhw\\_flat\\_plate.htm](http://www.flasolar.com/active_dhw_flat_plate.htm)>, March 2009
- [13] H.P. Garg, J. Prakash, 2000, Solar Energy, Fundamentals and applications, Tata McGraw Hill Publishing, ISBN 0-07-463631-6.
- [14] Alan Wyatt, 1986, Electric Power: Challenges and Choices. Book Press Ltd, ISBN 0-920650-00-7

- [15] Padki M, Sherif S, 1999, International Journal of Energy Research, 23, pg 249.
- [16] C.T. Crowe et al, 2005, Engineering fluid mechanics, 8th edition, John Wiley & Sons
- [17] Michael Modest, 2003, Radiative heat transfer, Amsterdam : Academic Press, Oxford Universiti Press.
- [18] S. Mathew, 2006, Wind Energy : Fundamentals, resource analysis and economics, Springer Publications, ISBN 3-540-30905-5.
- [19] G.L. Thomas, 2009, [www.cheresources.com](http://www.cheresources.com), Iterations for Colebrook equations.

# APPENDICES

Figure chart  
of  
factor,



A: Moody  
for  
calculation  
frictional  
 $f$ .

## NOMENCLATURES

Symbols	Units	Description
$\rho_{fg}$	kg/m <sup>3</sup>	Flue gas density at 850 K
$C_{p,fg}$	J/kg.K	Specific heat of flue gases at 850 K
$\mu_{fg}$	kg/m.s	Viscosity of flue gases at 850 K
$k$	W/m.K	Thermal conductivity of material
$Pr$	-	Prandtl number
$A_c$	m <sup>2</sup>	Inlet cross sectional area
$D_H$	m	Hydraulic diameter
$P$	m	Wetted parameter
$\dot{m}$	kg/s	Mass flow rate
$Re$	-	Reynolds number
$\epsilon$	-	Relative roughness
$f$	-	Frictional factor
$h$	W/m <sup>2</sup> K	Convection heat transfer coefficient
$Nu$	-	Nusselt's number
$N$	-	Number of fins
$A_b$	m <sup>2</sup>	Prime surface (base area)
$W$	m	Fin width
$L$	m	Fin length
$t$	m	Fin thickness
$A_f$	m <sup>2</sup>	Surface area of a fin
$A_t$	m <sup>2</sup>	Total area
$T_i$	K	Inlet flue gas temperature
$T_e$	K	Outlet flue gas temperature
$T_m$	K	Mean flue gas temperature
$T_p$	K	Plate temperature
$\theta_b$	K	Temperature distribution
$q_f$	W	Heat transfer of one fin
$q$	W	Heat transfer without fins

$\gamma_f$	-	Efficiency of a fin
$\gamma_o$	-	Overall fin efficiency
$q_t$	W	Total heat transfer of fins and base
$V_i$	m/s	Air velocity at inlet
$V_e$	m/s	Warm air velocity at exit
$V_{avg}$	m/s	Mean velocity
$A_i$	m <sup>2</sup>	Cross sectional area of inlet
$A_e$	m <sup>2</sup>	Cross sectional area of outlet
$g$	m/ s <sup>2</sup>	Gravitational acceleration
$K_c$	-	Constants for minor losses (fittings)
$C_p$	-	Power coefficient of rotors
$m_{air}$	kg/s	Mass flow rate of air
$H_{friction}$	m	Head losses due to friction in conduits
$H_{rotor}$	m	Head losses due to rotor
$H_{minor}$	m	Head losses due to change in shapes (fittings)
$T_{air.out}$	K	Temperature of air at the air outlet.
$T_{air.in}$	K	Temperature of air at the air inlet.
$T_{plate.out}$	K	Temperature of plate near the outlet.
$T_{plate.in}$	K	Temperature of plate near the inlet.
$V_{in}$	m/s	Velocity of air at the air inlet.
$V_{out.1}$	m/s	Velocity of air before the rotor.
$V_{out.2}$	m/s	Velocity of air after the rotor.
$I$	W/m <sup>2</sup>	Intensity of light in the atmosphere
$I_{\tau}$	W/m <sup>2</sup>	Intensity of light in the model (after perspex layer)